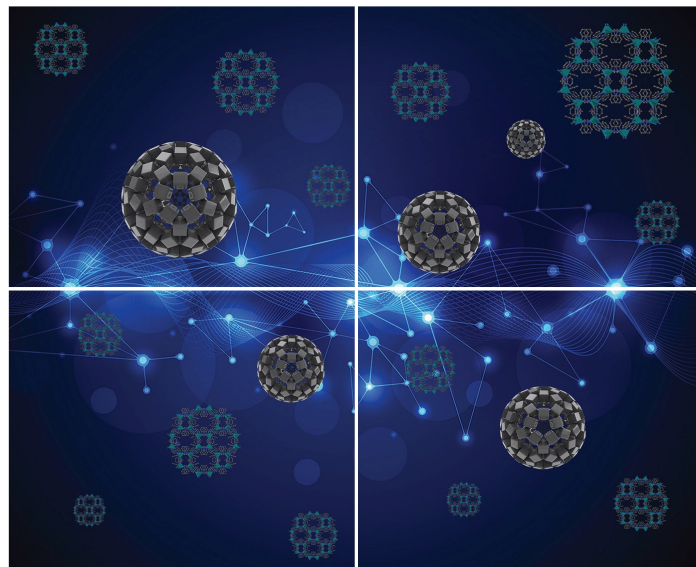


# INORGANIC CHEMISTRY

## FRONTIERS

Accepted Manuscript



This article can be cited before page numbers have been issued, to do this please use: L. de Cremoux, E. Falcone, D. Schmitt, E. Stefaniak, M. D. Wisniewska, N. Vitale, W. Bal and C. Hureau, *Inorg. Chem. Front.*, 2025, DOI: 10.1039/D5QI00850F.



This is an Accepted Manuscript, which has been through the Royal Society of Chemistry peer review process and has been accepted for publication.

Accepted Manuscripts are published online shortly after acceptance, before technical editing, formatting and proof reading. Using this free service, authors can make their results available to the community, in citable form, before we publish the edited article. We will replace this Accepted Manuscript with the edited and formatted Advance Article as soon as it is available.

You can find more information about Accepted Manuscripts in the [Information for Authors](#).

Please note that technical editing may introduce minor changes to the text and/or graphics, which may alter content. The journal's standard [Terms & Conditions](#) and the [Ethical guidelines](#) still apply. In no event shall the Royal Society of Chemistry be held responsible for any errors or omissions in this Accepted Manuscript or any consequences arising from the use of any information it contains.

## Modulation of A $\beta$ <sub>1-40</sub> and A $\beta$ <sub>4-40</sub> co-assembly by Zinc: getting closer to the biological reality

Lucie de Cremoux,<sup>[a]</sup> Enrico Falcone,<sup>[a]</sup> David Schmitt,<sup>[a,c]</sup> Ewelina Stefaniak,<sup>[a,b]</sup> Marta D. Wiśniewska,<sup>[b]</sup> Nicolas Vitale,<sup>[c]</sup> Wojciech Bal,<sup>[b]</sup> Christelle Hureau<sup>[a],\*</sup>

<sup>[a]</sup> CNRS, LCC (Laboratoire de Chimie de Coordination), 205 route de Narbonne, BP 44099, 31077 Toulouse Cedex 4 (France)

<sup>[b]</sup> Institute of Biochemistry and Biophysics, Polish Academy of Sciences, Pawińskiego 5a, 02-106 Warsaw Poland

<sup>[c]</sup> Centre National de la Recherche Scientifique, Université de Strasbourg, Institut des Neurosciences Cellulaires et Intégratives, F-67000 Strasbourg, France

**Abstract.** Alzheimer's disease (AD), one of the most common neurodegenerative diseases worldwide, is characterised by the self-assembly of amyloid- $\beta$  peptides (A $\beta$ ) in senile plaques, which are also rich in metal ions such as Cu and Zn. Here, we investigated the influence of Zn(II) ions on the self- and co-assembly of A $\beta$ <sub>1-40</sub> and the N-terminally truncated A $\beta$ <sub>4-40</sub> peptides, the two most prevalent A $\beta$  peptides in the brain. The Zn(II) coordination site in the soluble model peptide A $\beta$ <sub>4-16</sub> was investigated for the first time through pH-dependent X-ray absorption spectroscopy and nuclear magnetic resonance measurements, suggesting the formation of two species around neutral pH, depending on the (de)protonation of the N-terminal amine. The Zn(II) affinity was assessed via robust competition experiments, showing that A $\beta$ <sub>4-16</sub> has a four-fold lower affinity than A $\beta$ <sub>1-16</sub>. The self-assembly of A $\beta$ <sub>1-40</sub> and A $\beta$ <sub>4-40</sub>, and their co-assembly were monitored in presence of various Zn(II) levels, which reveals an important concentration-dependent modulatory effect of Zn(II) ions. In particular, the interplay between Zn(II), A $\beta$ <sub>1-40</sub> and A $\beta$ <sub>4-40</sub>, compared to either binary Zn-A $\beta$ <sub>x-40</sub> systems, promotes the formation of ill-defined assemblies regarded as more toxic than fibrils. This study provides new more-biologically relevant insights on the complex interaction between Zn(II) ions and the two major forms of A $\beta$  peptides detected in the senile plaques, underscoring their significance in the pathophysiology of AD.



## Introduction

View Article Online  
DOI: 10.1039/D5QI00850F

Alzheimer's disease (AD) is one of the most common neurodegenerative diseases worldwide, affecting an ever-increasing number of patients, with nearly 140 million predicted cases in 2050. AD is characterised by memory loss, behaviour and physical issues due to brain deterioration.<sup>1-3</sup> According to the amyloid cascade hypothesis,<sup>4-7</sup> the formation of extracellular deposits of amyloid- $\beta$  (A $\beta$ ) peptides is a direct cause of AD. Metal ions such as iron, copper and zinc are known to colocalize with amyloid deposits in AD brain at up to mM level.<sup>8-11</sup>

A $\beta$  peptides are intrinsically disordered peptides<sup>12</sup> of up to 42 amino-acid residues. Their sequences can be divided into two main parts: the N-terminal part (residues form 1 to 16) that is hydrophilic and involved in the coordination of metal ions,<sup>13-16</sup> and the C-terminal sequence (residues form 17 to 42) that is hydrophobic and involved in A $\beta$  self-assembly.<sup>17-19</sup> This process, commonly referred to as aggregation, results in the formation of highly structured fibrils enriched with cross- $\beta$  sheet structures, which eventually accumulate to form the senile plaques found in the brain of AD patients.<sup>10, 20-22</sup> This process is a supramolecular polymerisation that follows a nucleation and an elongation steps.<sup>23-31</sup> Secondary nucleation processes are also at play,<sup>23, 24, 32</sup> that can be either peptide-dependent (fibrils catalysed nucleation)<sup>24</sup> or independent (fibrils fragmentation) (**Scheme S1**). When two peptides are at play, the co-assembly occurs along different paths as reported for a few A $\beta$ -based peptides couples.<sup>33-36</sup> The most studied forms of A $\beta$  peptides are the A $\beta_{1-40}$  and A $\beta_{1-42}$  (sequence: <sup>1</sup>DAEFRHDSGYEVHHQKLVFFAEDVGSNKGAIIGLMVGGVVIA<sup>42</sup>), which originate from the proteolysis of the Amyloid Precursor Protein (APP).<sup>37, 38</sup> Although A $\beta_{1-42}$  is regarded as more toxic than A $\beta_{1-40}$  due to its larger aggregation propensity, it represents less than 5 % of the of amyloid-based material in deposits in contrast to A $\beta_{1-40}$  that is the predominant form.<sup>39-41</sup> However, it has been shown that A $\beta$  peptides belong to a larger family composed of several other forms including truncated and post-translationally modified variants.<sup>42-46</sup> The N-terminally truncated A $\beta$  peptides bearing the Phe4 at the N-terminal position (A $\beta_{4-x}$ ) were co-discovered with A $\beta_{1-x}$  as two major types of senile plaque components, in similar amounts.<sup>47, 48</sup> Later studies indicated that amounts of A $\beta_{4-42}$  and A $\beta_{1-42}$  in brain tissues are similar.<sup>43, 46, 49-52</sup> A $\beta_{4-x}$  is formed from the corresponding A $\beta_{1-x}$  by Zn proteases, prominently insulin-degrading enzyme,<sup>53, 54</sup> and neprilysin,<sup>55, 56</sup> which are also involved in general A $\beta$  catabolism. A $\beta_{4-42}$  was shown to display similar or higher toxicity levels than A $\beta_{1-42}$ ,<sup>49</sup> consistently with a higher propensity to assemble.<sup>57-59</sup>

In line with the high levels of metal ions found in amyloid plaques, a dysregulation of copper and zinc homeostasis that promotes pathological effects was reported in AD, in line with the possibility of copper and zinc(II) ions (hereafter noted as Zn) to bind to the A $\beta$  peptides at neutral pH.<sup>13, 16, 60-68</sup> As the redox-active Cu ion cycles between Cu(I) and Cu(II) redox states in biological media,<sup>69</sup> Cu-bound A $\beta$  peptides can be involved in the production of reactive oxygen species (ROS) contributing to the oxidative stress observed in AD.<sup>62, 70, 71</sup> In addition, Cu(II) or Zn(II) interactions with A $\beta_{1-40/42}$  impact its self-assembly.<sup>16, 63, 72-76</sup> Several studies described metal-induced modifications of A $\beta_{1-40}$  or A $\beta_{1-42}$  self-assemblies kinetics and of the morphology of the resulting fibrils.<sup>77-84</sup> Cu and Zn differently affect A $\beta$  self-assembly in line with their different binding sites.<sup>16, 72, 85</sup> In addition, the impact of a given metal ion depends on the sequence of the peptide at play due to distinct coordination sites and affinity. For instance, it has been shown that sub-stoichiometric ratio of Cu has significantly weaker impact on the kinetics of A $\beta_{4-40}$  self-assembly compared to that of A $\beta_{1-40}$ , although for both peptides, Cu enhanced the formation of amorphous aggregates at super-stoichiometric ratios.<sup>19</sup> In contrast to Cu, Zn cannot bind to the FRH ATCUN motif found in A $\beta_{4-40}$ , which involves the N-terminal amine, the imidazole group of the His at the third position and the two deprotonated amide in-between.<sup>86, 87</sup> Indeed, Zn is generally not able to induced the deprotonation of amide due to its lower Lewis acidic character compared to



Cu(II)).<sup>88, 89</sup> The Zn coordination to A $\beta$ <sub>4-40</sub> and resulting effects on self-assembly are still barely studied, although Zn is one of the most abundant metal ions in the brain<sup>60, 68, 90, 91</sup> (10 to 100-fold more abundant than Cu).

With the long-term objective to better understand the impact of Zn metal ions in the amyloid cascade linked to AD, we have first determined the Zn binding properties of A $\beta$ <sub>4-40</sub>, knowing that Zn binding to A $\beta$ <sub>1-40</sub> is well documented.<sup>92-100</sup> Coordination mode(s) of Zn and its affinity for the A $\beta$ <sub>4-x</sub> peptide have thus been evaluated near neutral pH. Then, the impact of Zn on the self-assembly of either A $\beta$ <sub>1-40</sub> or A $\beta$ <sub>4-40</sub> was investigated to reveal peptide-specific Zn-modulated self-assembly trends. Furthermore, the effect of Zn on the co-assembly of the biologically relevant A $\beta$ <sub>1-40</sub>/A $\beta$ <sub>4-40</sub> (1/1) mixture was also evaluated. This will give insights into a three components assembly involving one metal and two peptides whereas most studies have focused on only one component (peptide) or two components (two peptides or a peptide + a metal) assembly.



## Results and discussion

View Article Online  
DOI: 10.1039/D5QI00850F

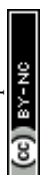
Due to the propensity of  $\text{Zn}(\text{A}\beta_{x-40})$  to aggregate, the studies on Zn coordination sites and affinity were performed with the C-terminally truncated model peptides encompassing the residues 1 to 16 and 4 to 16 (with both the COOH and  $\text{CONH}_2$  as the C-termini). These models are known to contain the main binding residues of the full-length peptides,<sup>13, 101</sup> but don't self-assemble at the concentration required for the spectroscopic studies.

### pH-dependent Zn coordination studies

We performed a pH-dependent study of Zn binding to the C-terminally truncated peptides  $\text{A}\beta_{4-16}\text{-COOH/-CONH}_2$  using XAS (X-ray Absorption Spectroscopy) and NMR spectroscopies and compared the data with those of related peptides, mainly  $\text{A}\beta_{1-16}$ . The investigation of the coordination site in a fairly large pH range (here from 6.8 to 8.2), rather than only at neutral pH, has proven to be a reliable strategy to better describe the coordination site of metal ions (Zn and Cu) at neutral pH, see e.g. refs.<sup>93, 102-106</sup> In order to study the pH-dependent speciation of  $\text{Zn}(\text{A}\beta_{4-16})$  complexes, potentiometric titrations have been attempted but have been impaired by the gradual precipitation and poor solubility of  $\text{Zn}(\text{A}\beta)$  complexes at the concentration (ca. mM) required for such measurements, in line with previous reports.<sup>107, 108</sup> Only the protonation constants of  $\text{A}\beta_{1-16}$  and  $\text{A}\beta_{4-16}$  were re-evaluated (**Tables S1** and **S2**).

### X-ray absorption spectroscopy

The coordination site of Zn bound to the  $\text{A}\beta_{4-16}\text{-CONH}_2$  peptide was first studied by XAS, which is the method of choice for  $d^{10}$  ions, silent in most classical spectroscopy.<sup>109-111</sup> XAS spectra of  $\text{Zn}(\text{A}\beta_{4-16}\text{-CONH}_2)$  were recorded at physiological pH 7.4, and at pH 6.9 and 7.9 to probe a possible pH-dependent Zn coordination to the  $\text{A}\beta_{4-16}\text{-CONH}_2$  peptide. In the K-edge XANES (X-ray Absorption Near Edge Structure) spectra of Zn bound to  $\text{A}\beta_{4-16}\text{-CONH}_2$  recorded at these three pH values (coloured traces, Figure 1.A), the white line intensity (i.e. intensity at  $\approx 9666$  eV) – which correlates with the Zn coordination number – is in line with a tetragonal Zn centre (**Table S3**),<sup>110</sup> as reported earlier for Zn bound to  $\text{A}\beta$  peptides of various sequences including  $\text{A}\beta_{1-16}\text{-CONH}_2$  (black trace, Figure 1).<sup>92, 93, 101, 112</sup> In addition, the recorded signatures were mostly free of unbound Zn (**Figure S1**) and pH-dependent, as previously reported for the  $\text{Zn}(\text{A}\beta_{1-16})$  complex.<sup>93, 112</sup> The EXAFS (Extended X-ray Absorption Fine Structure) spectra of Zn bound to  $\text{A}\beta_{4-16}\text{-CONH}_2$  at the three pH values (coloured traces, **Figure 1.B**) were virtually identical to each other and displayed a bimodal interference pattern between  $k \approx 3$  and  $5 \text{ \AA}^{-1}$  (grey region, **Figure 1.B**) typical of multiple-scattering contributions from outer shells of His imidazole rings.<sup>113</sup> This reveals the involvement of His residues in the coordination sphere of  $\text{Zn}(\text{A}\beta_{4-16}\text{-CONH}_2)$  throughout the pH range explored (6.9-7.9). Moreover, the EXAFS spectra of  $\text{Zn}(\text{A}\beta_{4-16}\text{-CONH}_2)$  are indistinguishable from that of  $\text{Zn}(\text{A}\beta_{1-16}\text{-CONH}_2)$ , for which a tetragonal sites with 4 N/O ligands including 2 His residues was proposed (note that N and O ligands are not distinguishable by EXAFS).<sup>114</sup> Hence, based on the similarity between the XAS spectra of  $\text{Zn}(\text{A}\beta_{4-16})$  and  $\text{Zn}(\text{A}\beta_{1-16})$ , an analogous tetragonal site including 2 His and 2 O ligands is inferred for  $\text{Zn}(\text{A}\beta_{4-16}\text{-CONH}_2)$ .



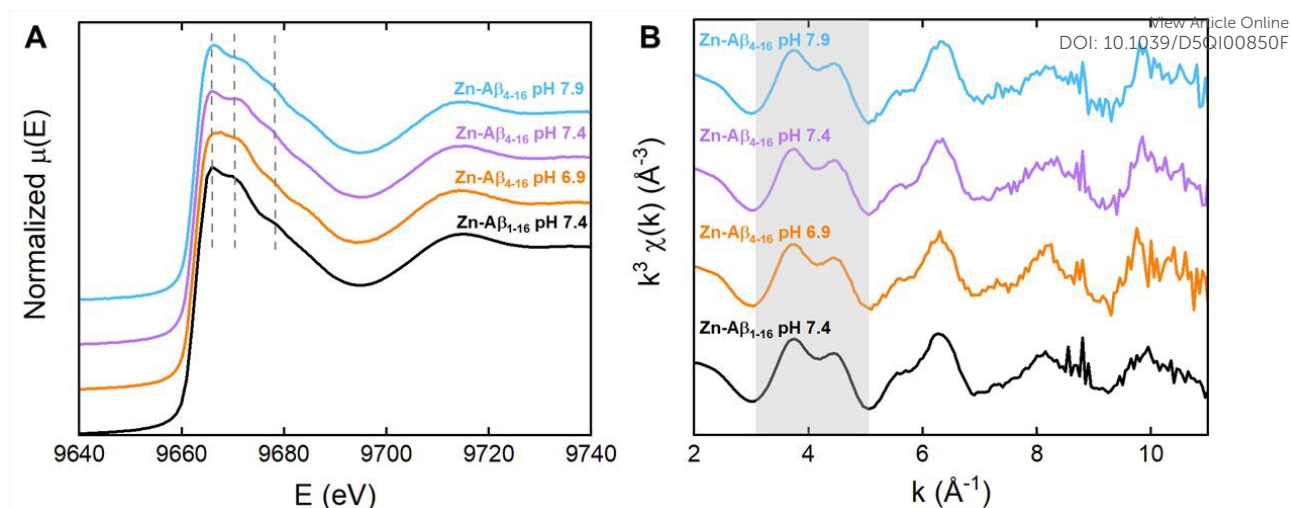


**Figure 1.** XAS spectra of Zn(A $\beta_{4-16}$ ) at pH 6.9 (orange), pH 7.4 (purple) and pH 7.9 (blue) compared to Zn(A $\beta_{1-16}$ ) at pH 7.4 (black). (A) normalized K-edge XANES spectra; (B)  $k^3$ -weighted EXAFS spectra. Conditions: [A $\beta$ ] = 1.2 mM, [Zn] = 1 mM, [HEPES] = 100 mM. Glycerol (10% v/v) was used as a cryoprotectant, T = 10 K. In (B), the grey region ( $k \approx 3-5 \text{ \AA}^{-1}$ ) highlights the bimodal interference pattern due to multiple scattering from imidazole rings.

### NMR spectroscopy

To further investigate the Zn coordination sites within the A $\beta_{4-x}$  peptides, pH-dependent  $^1\text{H}$  NMR experiments were performed (**Figure 2**, where data are shown at 0.5 equiv. of Zn for matter of clarity; for the complete range of ratio, see **Figure S3-S4**). Detection of the groups interacting with Zn can indeed be achieved by studying the effect of the Zn addition on the NMR proton signals. Zn binding usually results in the changes of chemical shifts, accompanied by moderate line broadening of the signals of protons neighbouring the binding site.<sup>92-94, 97, 99, 108</sup> In the present case, Zn addition to the A $\beta_{4-16}$  peptide led to a broadening of the NMR spectra regardless of the pH values (**Figure 2**). This is due to the combination of (i) a residue-specific broadening resulting from the interaction between the Zn and the peptide in a fast exchange regime,<sup>99</sup> and (ii) a residue-unspecific broadening imputable to the precipitation of Zn(A $\beta_{4-16}$ ) that increases with pH and over time.





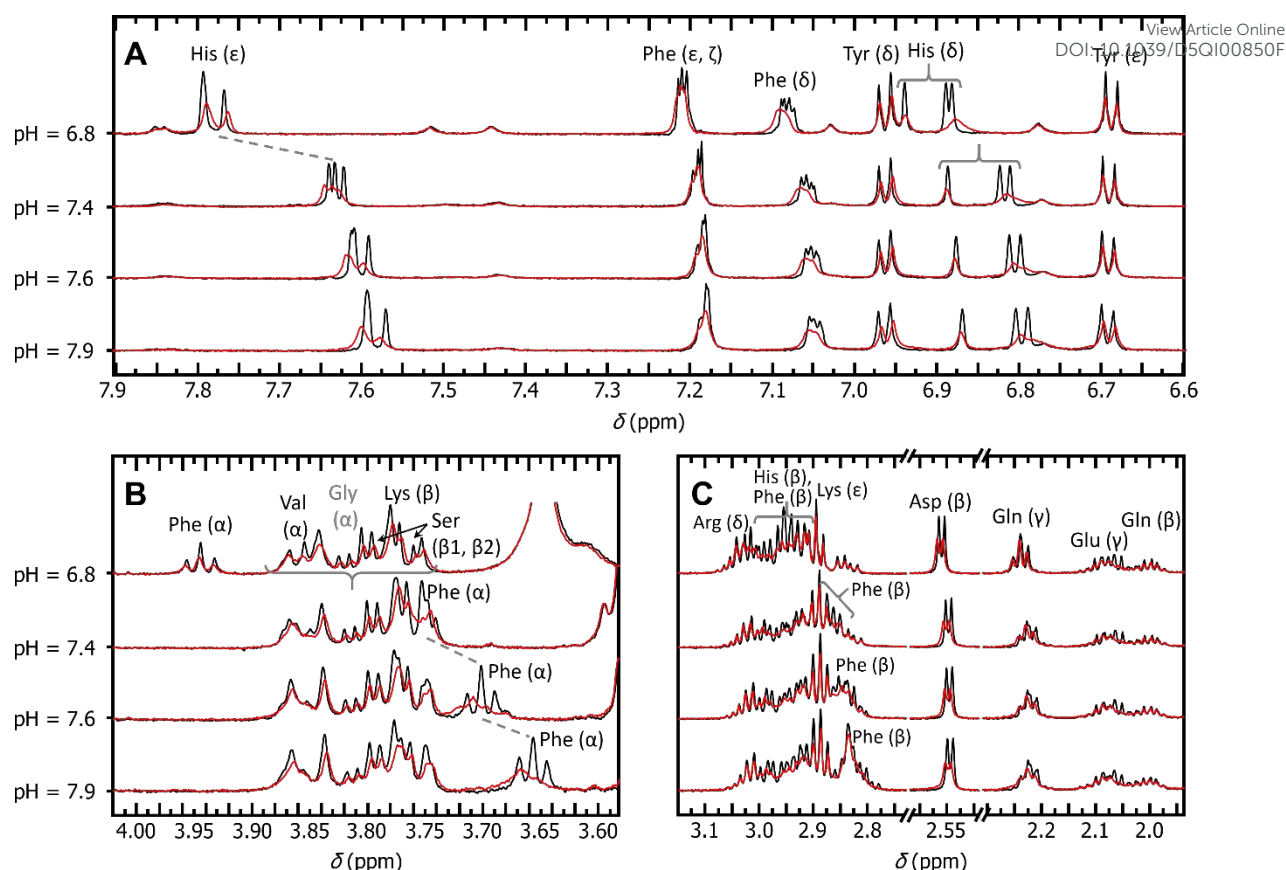


**Figure 2.**  $^1\text{H}$  NMR spectra of  $\text{A}\beta_{4-16}$  peptide in the absence (black) or presence of 0.5 eq. Zn (red) at different pH. Panels A, B, C show the following spectral regions: A, 7.9–6.6 ppm; B, 4–3.6 ppm; C, 3.1–1.9 ppm). Conditions:  $[\text{A}\beta] = 200 \mu\text{M}$ ,  $[\text{Zn}] = 100 \mu\text{M}$ ,  $[\text{d}_{19}\text{-Bis-tris}] = 50 \text{ mM}$ , 10%  $\text{D}_2\text{O}$ , in milliQ water, pH = 6.8, 7.4, 7.6 or 7.9,  $T = 298\text{K}$ ,  $\nu = 600 \text{ MHz}$ . The assignment of  $^1\text{H}$  chemical shifts of  $\text{A}\beta_{4-16}$  peptide was achieved by TOCSY experiments (Figure S2, Tables S3 and S4).

In the aromatic region, the different protons of the His were impacted by the addition of Zn on the  $\text{A}\beta_{4-16}$  peptide by both a change in the chemical shifts and a broadening (Figure 2.A). The signals of the aromatic protons of Phe4 and Tyr10 were much less broadened than those of His, and the Phe4 ( $\text{H}_\delta$ ) was slightly shifted downfield at all pH values. The impact of Zn on the Phe4 aromatic signals, observed to a larger extent at higher pH values, was stronger than those previously reported for a series of  $\text{A}\beta_{1-16}$  peptides.<sup>92, 93</sup>

Furthermore, the  $\text{H}_\alpha$  signal of the N-terminal Phe4 of  $\text{A}\beta_{4-16}$  was strongly shifted upfield with the increase of the pH values (Figure 2.B), in line with deprotonation of the amine near pH 7.6 (as evaluated by potentiometry, see Table S2). The presence of Zn induced a downshift and a broadening of this signal at all pH values, whose extent increases with pH. Altogether, the effect of Zn on Phe4 signals may indicate that Zn binding to the N-terminal amine occurs between pH 6.8 (weak effects) and pH 7.9 (strong effects), in line with the deprotonation of the N-terminal amine.

The proton signals of the Asp7  $\text{H}_\beta$  and Glu11  $\text{H}_\gamma$  were weakly broadened by the addition of Zn ions regardless of pH (Figure 2.C), indicating the possible participation of these amino-acid residues in Zn binding. It is worth noting that the impact of Zn on the carboxylate-containing residues was weaker in case of the  $\text{A}\beta_{4-16}\text{-COOH}$  versus  $\text{A}\beta_{4-16}\text{-CONH}_2$  in the whole pH range tested (compare Figures S3 and S4) suggesting that the non-biologically relevant C-terminal carboxylate participates in the Zn binding, entering in competition with those of Asp7 and Glu11 side-chains. In addition, the Val12  $\text{H}_\gamma$  was



significantly affected by Zn addition regardless of the pH (**Figures S3-S4**). Such feature was not observed for E11Q- and H13A-A $\beta_{1-16}$  mutants,<sup>92</sup> which suggests the involvement of both Glu11 and His13 in Zn binding to the A $\beta_{4-16}$  peptide.

### Zn-binding affinity

The affinity of Zn(A $\beta$ ) complexes was then studied by a robust competition assay relying on the use of a water-soluble chelator N,N'-Bis[(5-sulfonato-2-hydroxy)benzyl]-N,N'-dimethyl-ethane-1,2-diamine (also called L<sub>2</sub>) previously described (**Figure S5**).<sup>115</sup> The competition experiments were realised following the absorbance of the characteristic band of the Zn(L<sub>2</sub>) complex, corresponding to the phenolate to Zn charge transfer transition in Zn(L<sub>2</sub>), at 254 nm, by UV-vis spectroscopy. The experimental absorbance of the Zn(L<sub>2</sub>) complex was studied as a function of peptide concentration for A $\beta_{1-16}$  and A $\beta_{4-16}$  (both C-terminal free and C-amidated peptides). A $\beta$  peptides were able to remove competitively the Zn ions from the Zn(L<sub>2</sub>) complex leading to the formation of Zn(A $\beta$ ). Indeed, the addition of the A $\beta$  peptides to the Zn(L<sub>2</sub>) complex led to the disappearance of its characteristic band at 254 nm (**Figures 3.A** and **S6**), and to the appearance of a band at 275 nm corresponding to the absorbance of the Tyr10 from the peptides (**Figure S7**). The reproduction of the experimental normalized curves corresponding to the absorbance at 254 nm as a function of the concentration of peptide added (**Figure 3.B**) was realised following a previously described *in-house* procedure<sup>115</sup> (see experimental part for details).

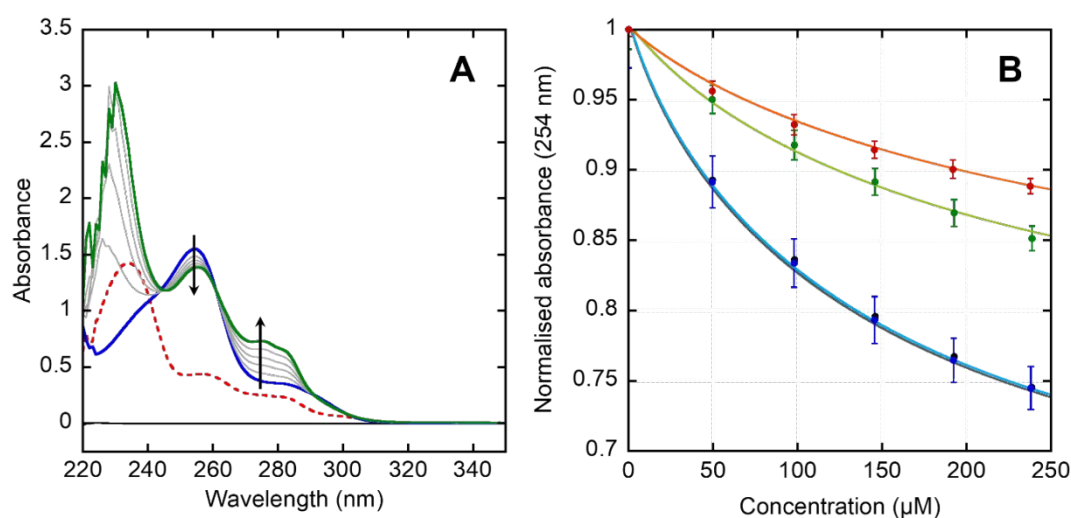


**Figure 3.** (A) UV-Vis spectra of a solution of L<sub>2</sub> (red dotted line), in the presence of Zn ions (blue), and with the addition of increasing concentrations of A $\beta_{4-16}$ -CONH<sub>2</sub> peptide (grey to green lines). The arrows indicate the variation of the bands of the Zn(L<sub>2</sub>) complex upon A $\beta$  addition. (B) Normalised experimental absorbance (dots) and their best fit (lines) of the competition between Zn(L<sub>2</sub>) and increasing concentration of A $\beta_{1-16}$ -COOH (black), A $\beta_{1-16}$ -CONH<sub>2</sub> (blue), A $\beta_{4-16}$ -COOH (green), A $\beta_{4-16}$ -CONH<sub>2</sub> (red) peptides. Conditions: [L<sub>2</sub>] = 60  $\mu$ M, [Zn] = 50  $\mu$ M, [A $\beta$ ] = 50 to 250  $\mu$ M, [HEPES] = 50 mM, pH = 7.1, T = 25°C. Average of two experiments.

All the experimental data have been well reproduced based on the formation of a 1:1 Zn:peptide complex. The apparent association constant of Zn(A $\beta_{1-16}$ -COOH) and Zn(A $\beta_{1-16}$ -CONH<sub>2</sub>) results to be  $K_{app} = 1.1 \cdot 10^5 \text{ M}^{-1}$  (**Table 1**) in line with data obtained using various methods<sup>93, 96, 100, 108, 115</sup> and taking the apparent affinity of Zn for L<sub>2</sub> at  $1.2 \cdot 10^6 \text{ M}^{-1}$  at pH 7.1.<sup>115</sup> The data for both A $\beta_{1-16}$ -COOH and A $\beta_{1-16}$ -CONH<sub>2</sub> peptides are virtually identical, indicating that the C-term protection of the A $\beta_{1-16}$  sequence has no impact on the Zn affinity for the A $\beta_{1-16}$ .





The N-truncation at position 4 of the A $\beta$  peptides induced a significant decrease of the Zn affinity, with values of  $K_{app} = 4.5 \cdot 10^4 \text{ M}^{-1}$  and a  $K_{app} = 2.5 \cdot 10^4 \text{ M}^{-1}$  for A $\beta_{4-16}$ -COOH and A $\beta_{4-16}$ -CONH<sub>2</sub> (Table 1), respectively. This indicates that the formation of the Zn(A $\beta_{4-16}$ ) complex is disfavoured by the loss of the first three amino acid residues. This is consistent with the fact that Asp1 and Glu3 were proposed to be involved in Zn-binding in the A $\beta_{1-16}$  peptide.<sup>92</sup> A similar trend was observed for D1N, E11Q and to a lesser extent E3Q and D7N mutants of the A $\beta_{1-16}$ -COOH.<sup>92</sup> In contrast to the observation made on the A $\beta_{1-16}$ , the C-terminal protection of the A $\beta_{4-16}$  peptide leads to a two-fold decrease in the evaluated Zn affinity. This is in line with the participation of the non-biologically relevant C-terminal carboxylate in Zn binding within the A $\beta_{4-16}$ -COOH peptide and in line with the previous observations made by NMR. We surmise that the different response of A $\beta_{1-16}$  and A $\beta_{4-16}$  to the C-term protection may arise from a combination of the following factors: i) the lower number of carboxylate groups in A $\beta_{4-16}$  relative to A $\beta_{1-16}$ , ii) the closer proximity to the C-terminus of the Zn-binding site in A $\beta_{4-16}$  relative to A $\beta_{1-16}$ , iii) the overall less negative charge of A $\beta_{4-16}$  relative to A $\beta_{1-16}$ . In brief, the affinity measured by the competition experiments indicates an affinity of about  $10^5 \text{ M}^{-1}$  at neutral pH, with a higher affinity for A $\beta_{1-16}$  versus A $\beta_{4-16}$  in line with the presence of two additional carboxylate-containing residues at positions 1 and 3 in the former peptide.

**Table 1.** Apparent Zn affinity values for the two peptides under study here.

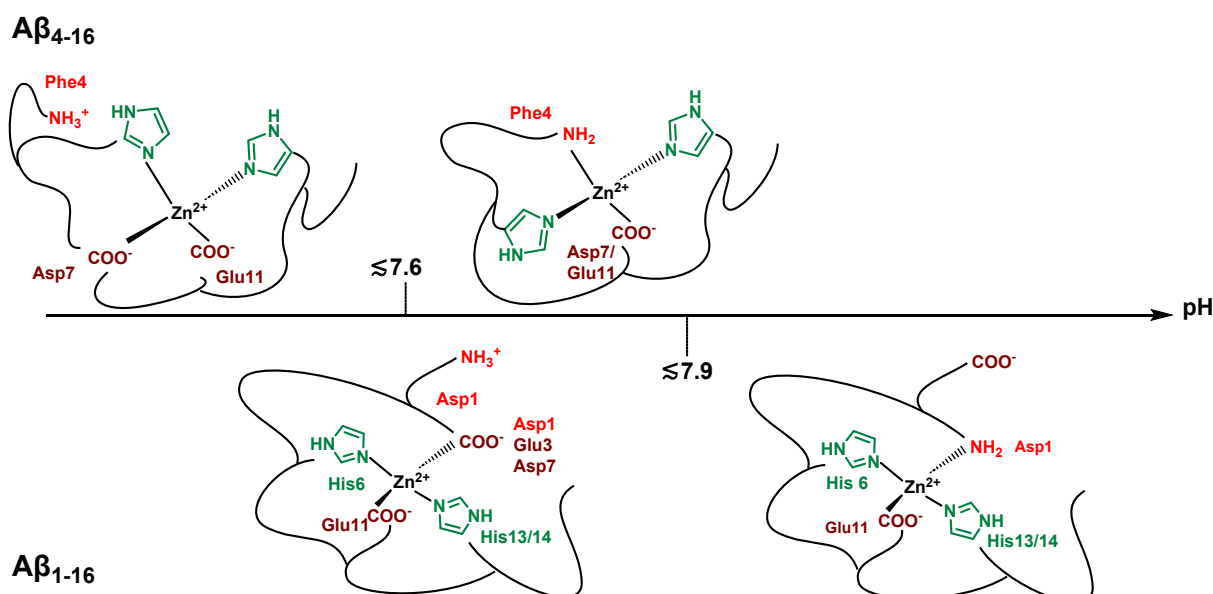
Peptide	$K_{app} (10^5 \text{ M}^{-1})$ at pH 7.1
A $\beta_{1-16}$ -COOH	1.1 $\pm$ 0.1
A $\beta_{1-16}$ -CONH <sub>2</sub>	1.1 $\pm$ 0.1
A $\beta_{4-16}$ -COOH	0.45 $\pm$ 0.1
A $\beta_{4-16}$ -CONH <sub>2</sub>	0.25 $\pm$ 0.1

### Zn coordination sites in A $\beta_{4-16}$ -CONH<sub>2</sub>

Based on the results described above and the reported Zn binding sites in related A $\beta$  peptides,<sup>92, 93</sup> we propose the Zn coordination sites to A $\beta_{4-16}$ -CONH<sub>2</sub> shown in Scheme 1, top. This coordination is pH-dependent in line with the deprotonation of the N-terminal amine that further enters the Zn coordination sphere as evidenced by the stronger Zn-induced broadening of Phe4 resonances observed in NMR. At “low” pH, the main coordination site for the Zn(A $\beta_{4-16}$ ) complex is similar to the one proposed for the Zn(A $\beta_{1-16}$ ) reminded in Scheme 1, bottom.<sup>92, 93</sup> It is based on a [2N2O] site made of two imidazole groups from His and two carboxylate groups from Asp7 and Glu11 residues (Scheme 1, top). Similar to A $\beta_{1-16}$  coordination site, the two imidazole groups would be from two among the three His residues in equilibrium. On the Zn(A $\beta_{1-16}$ ) complex, a dynamic exchange between the Asp1, Glu3, and Asp7 was reported. As the A $\beta_{4-16}$  peptide is truncated at position 4, this exchange can’t be observed on the Zn(A $\beta_{4-16}$ ) complex as the two carboxylate groups are always bound to Zn. Besides, because the available potential carboxylate groups are only two, the possibility of having the three His bound cannot be fully ruled out, the last coordination position being then occupied by the side chains of Asp7 or Glu11 in exchange (Scheme S3). At “high” pH, the main coordination sites for the Zn(A $\beta_{4-16}$ ) complex are issued from those at “low” pH, taking into account the deprotonation of the amine and the resulting replacement of an imidazole or a carboxylate side-chain. Hence, a [3N1O] built on two imidazole rings from His residues, a carboxylate group (Asp7 or Glu11, in equilibrium) and the N-terminal amine of the peptide (Scheme 1, top) or a [2N2O] made by one imidazole from His residues, the two carboxylate groups (Asp7 and Glu11) and the N-terminal amine of the peptide (Scheme S1, top) are proposed. Considering that the EXAFS signatures are reminiscent of Zn-sites containing two imidazole groups,<sup>92, 93, 110</sup> the [2N2O] might be the favoured binding site at both low and high pH. It is also worth pointing out that, even though the peptide is highly flexible and can provide enough ligands to fill the tetragonal coordination sphere of Zn, the coordination of a water molecules cannot be ruled



out. Since, unlike Cu(II), Zn is not able to induce the deprotonation of the N-terminal amine, the  $pK_a$  of transition between the “low” and “high” pH species is lower but not too far from that of the deprotonation of the N-terminal amine in the apo-peptide, namely 7.6 (**Table S2**). Hence, in the case of Zn( $A\beta_{4-16}$ ), the deprotonation of N-terminal amine occurs at lower pH than in the case of Zn( $A\beta_{1-16}$ ). This is linked to the different  $pK_a$  of the terminal amine in the corresponding apo-peptides, which can be attributed to the possibility of stabilizing the protonated form of the amine due to a metallacycle with the carboxylate side-chain of Asp1 in the case of  $A\beta_{1-16}$  (**Scheme S4**). In addition, it is anticipated that the binding of the N-terminal amine to the Zn occurs at a lower pH in the case of  $A\beta_{4-16}$  since there are fewer potential binding residues compared to  $A\beta_{1-16}$ .



**Scheme 1.** Proposed coordination sites for Zn( $A\beta_{4-16}$ ) complex near physiological pH (top) compared to proposed coordination sites for Zn( $A\beta_{1-16}$ ) (bottom) from refs.<sup>92, 93</sup>.



## Zn impact on A $\beta$ self-assembly and co-assembly

View Article Online  
DOI: 10.1039/D5QI00850F

After having evaluated the coordination of Zn to the A $\beta_{4-16}$ -COOH/NH<sub>2</sub> model peptide, the impact of Zn on the self-assembly of A $\beta_{4-40}$  was compared to that of A $\beta_{1-40}$  in link with the different Zn binding site and affinity revealed for the two peptides. In addition, the modulation of the co-assembly of both peptides by different amounts of Zn is also described and discussed. The kinetics of the assemblies of A $\beta_{1-40}$  and A $\beta_{4-40}$  was monitored by the enhancement of the thioflavin T (ThT) fluorescence and key parameters evaluated (see Experimental section for details). The morphology of the fibrils at the end of the assembly process was evaluated by transmission electron microscopy (TEM). Six independent experiments were performed to secure the detection of reliable trends.<sup>116, 117</sup> A representative experiment is described below and the other ones are gathered in the Supporting Information (**Figures S9** and **S10**, and **Figures S11-S14** for additional TEM pictures); similar trends were detected. To ease the description and unless otherwise stated, the reported values correspond to the experiment shown in the full text, and the kinetic parameters corresponding to the other available experiments are given in **Tables S6-S7**.

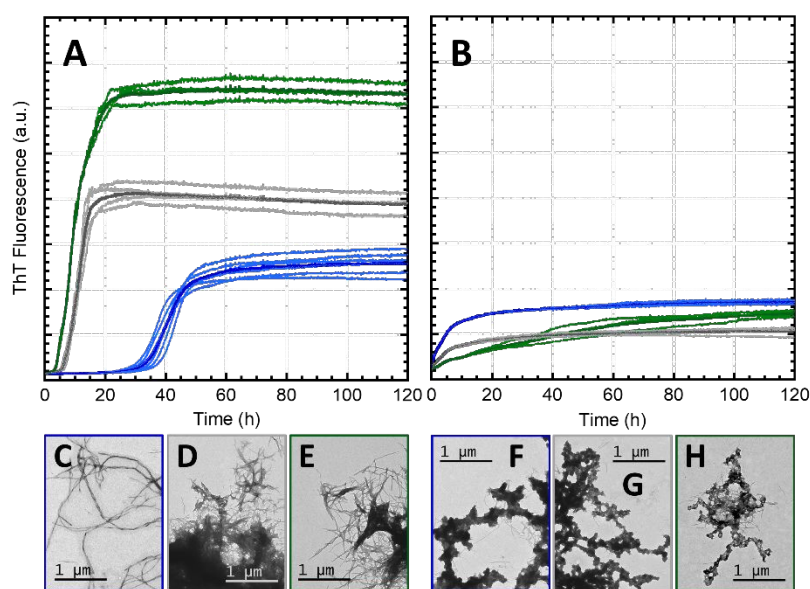


**Figure 4.** Selection of representative ThT curves of A $\beta$  peptides without (A) and with 1 equiv. of Zn (B): A $\beta_{1-40}$  (blue), equimolar mixture of A $\beta_{1-40}$  and A $\beta_{4-40}$  (grey), and A $\beta_{4-40}$  (green). The thin lines correspond to individual replicates and the bold lines to their average. The ThT fluorescence intensities are in arbitrary units and are plotted with the same scale to be directly comparable. Conditions: [A $\beta$ ]<sub>total</sub> = 20  $\mu$ M, [Zn] = 20  $\mu$ M, [ThT] = 10  $\mu$ M, [HEPES] = 100 mM, pH = 7.4, [EDTA] = 0.02  $\mu$ M, T = 37°C. Corresponding TEM pictures taken after 7 days of self-assembly of A $\beta_{1-40}$  (C and F), equimolar mixture of A $\beta_{1-40}$  and A $\beta_{4-40}$  (D and G), and A $\beta_{4-40}$  (E and H).

**Apo-peptides.** The self-assembly kinetics of A $\beta_{1-40}$  and A $\beta_{4-40}$  were first examined. A symmetric sigmoidal curve is observed in the case of the A $\beta_{1-40}$  peptide (blue curves in **Figure 4.A**) with a  $t_{1/2}$  of about 40 h and a growth rate  $k$  of about 0.3 h<sup>-1</sup> (See Experimental details for the description of kinetic parameters). TEM revealed that A $\beta_{1-40}$  fibrils are long with characteristic twists (**Figure 4.C**). In contrast, the self-assembly of the A $\beta_{4-40}$  was very fast ( $t_{1/2}$  < 10h), with an asymmetrical profile (green curves in **Figure 4.A**). A similar  $k$  to that of A $\beta_{1-40}$  was obtained by our in-house calculation procedure (note that visually the  $k$  of A $\beta_{4-40}$  seems higher than that of A $\beta_{1-40}$  due to the fact that the curves are not normalized). The  $t_{1/2}$  and  $k$  parameters obtained for A $\beta_{4-40}$  versus A $\beta_{1-40}$  indicate that the first nucleation step is faster in the case of A $\beta_{4-40}$  but not the growth phase. The final fluorescence intensity increase (



$\Delta F$ ) is about 2.5 times higher for  $A\beta_{4-40}$  versus  $A\beta_{1-40}$ . Note that the intensity of the ThT fluorescence depends on the quantity of fibrils but also on their morphology.<sup>118</sup> Furthermore,  $A\beta_{4-40}$  fibrils are shorter without any twists but stacked together (**Figure 4.E**). The co-assembly of an equimolar ratio of  $A\beta_{1-40}$  and  $A\beta_{4-40}$  was subsequently studied (grey curves in **Figure 4.A**). The  $t_{1/2}$  value of the mixture is close (**Table 2**) or even lower (**Table S5**) to the one obtained with  $A\beta_{4-40}$  (approx. 11 h). This indicates that the two peptides can also form heteronuclei. The curve is more symmetrical than that of  $A\beta_{4-40}$  and steeper than those of  $A\beta_{1-40}$  or  $A\beta_{4-40}$  ( $k = 0.48 \text{ h}^{-1}$ ), indicating that the elongation is faster in presence of both peptides, and hence further suggests that the two peptides co-assemble (**Scheme 2**, compare first reactions of each panel). The  $\Delta F$  value lies in between those of  $A\beta_{1-40}$  and  $A\beta_{4-40}$  and the morphology of the fibrils obtained with the 1:1 mixture corresponds to fibrils stacked together similarly as those observed for  $A\beta_{4-40}$  (**Figure 4.D**).<sup>57</sup>

**Holo-peptides.** Upon addition of one equivalent (later noted equiv.) of Zn, a strong decrease of the ThT fluorescence was observed for both peptides and their mixtures (**Figure 4.B**), in line with the formation of less structured assemblies as pictured by TEM (**Figure 4.F-H**). Note that we have also secured that Zn stay bound to the peptide upon aggregation. We have thus measured the distribution of Zn between the peptide aggregates and the supernatant using 4-(2-pyridylazo)resorcinol (PAR) as Zn-responsive chromophore (see Experimental Section for details and **Figure S15**).<sup>119</sup> The level of Zn is very low in the supernatant (< 20%). This suggests a slightly increased affinity for Zn bound to the aggregates versus the monomeric peptides. The relative affinity observed for the  $A\beta_{1-16}$  versus  $A\beta_{4-16}$  is also qualitatively found again within the corresponding peptides aggregates.

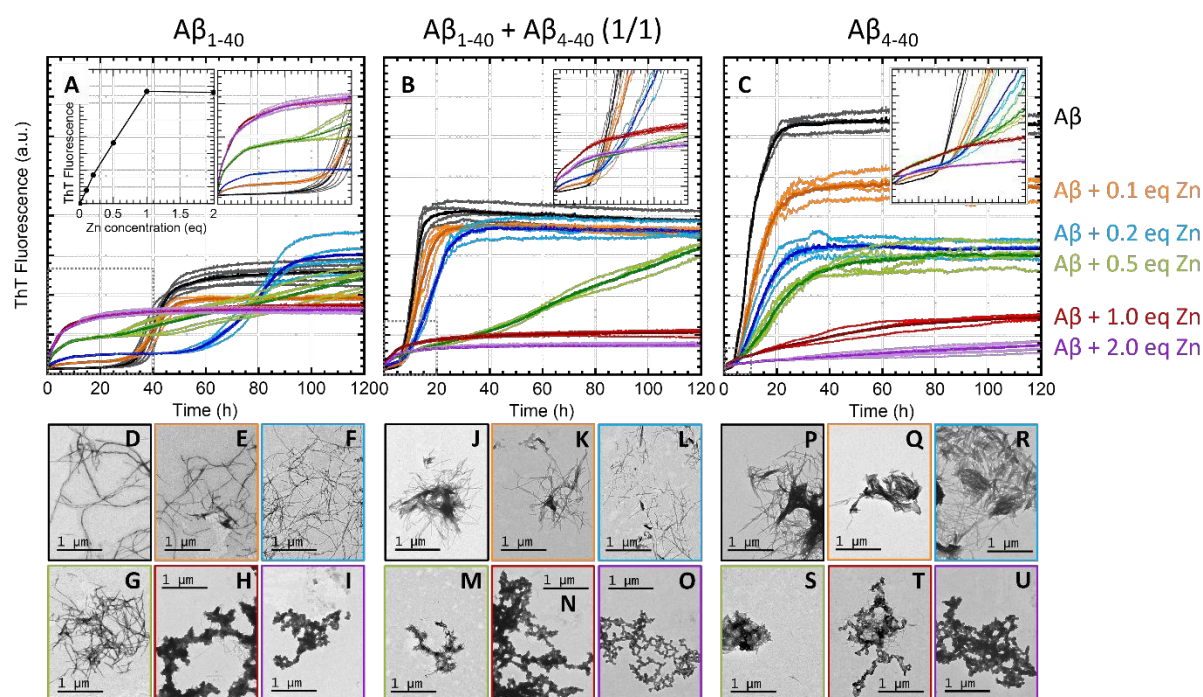


**Figure 5.** Selection of representative ThT curves of  $A\beta_{1-40}$  (A), equimolar mixture of  $A\beta_{1-40}$  and  $A\beta_{4-40}$  (B), and  $A\beta_{4-40}$  (C) with different concentrations of Zn: Apo (black),  $A\beta + 0.1 \text{ equiv. Zn}$  (orange),  $A\beta + 0.2 \text{ equiv. Zn}$  (blue),  $A\beta + 0.5 \text{ equiv. Zn}$  (green),  $A\beta + 1 \text{ equiv. Zn}$  (red) and  $A\beta + 2 \text{ equiv. Zn}$  (purple). Insets correspond to the first hours of the assembly experiments (highlighted by the dotted boxes in each panel). For panel A, the second inset corresponds to the ThT value after the first increase as a function of the equiv. of Zn. The thin lines correspond to the replicates and the bold ones to the average of the replicates. The ThT fluorescence intensities are in arbitrary units and are plotted with the same scale to be directly comparable. Conditions:  $[A\beta]_{\text{total}} = 20 \mu\text{M}$ ,  $[Zn] = 2, 4, 10, 20 \text{ or } 40 \mu\text{M}$ ,  $[ThT] = 10 \mu\text{M}$ ,  $[HEPES] = 100 \text{ mM}$ ,  $\text{pH} = 7.4$ ,  $[EDTA] = 0.02 \mu\text{M}$ ,  $T = 37^\circ\text{C}$ . Corresponding TEM pictures taken after 7 days of self-assembly of  $A\beta_{1-40}$  (D-I), equimolar mixture of  $A\beta_{1-40}$  and  $A\beta_{4-40}$  (J-O), and  $A\beta_{4-40}$  (P-U); the coloured frameworks corresponds to the code used for the ThT curves.





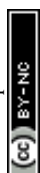
To gain deeper insights into the impact of Zn on the peptides' assembly, studies were performed at various ratios of Zn:peptide (from 0.1 to 2.0 equiv.). This was first studied on  $A\beta_{1-40}$  self-assembly (**Figure 5.A**). In the presence of Zn, a rapid fluorescence increase was observed, which is almost proportional to the Zn:peptide ratio up to 1 equiv. Zn (Inset in **Figure 5.A**). After the first ThT fluorescence plateau, a second process occurred, that is sigmoidal and observed up to 0.5 equiv. Zn. This trend is reminiscent of previous observations.<sup>120</sup> At 0.1 equiv. of Zn (orange curves), the  $t_{1/2}^*$  and the  $\Delta F^*$  values were similar than in absence of Zn (\* indicates that the second sigmoidal process is under focus). The time ( $t_{1/2}^*$ ) at which this second rise occurred increases with the Zn:peptide ratio (to about 60h at 0.5 equiv. Zn), while the slope  $k^*$  decreased (**Table 2**) and the final ThT value remained similar to that of apo- $A\beta_{1-40}$  (**Table S6**).

The morphology of the aggregates formed are shown in **Figure 5.E-G**. With increasing ratio of Zn, the fibrils became progressively shorter and without any visible twists. At 1.0 and 2.0 equiv. of Zn, only the first process was observed (**Figure 5.A**), and large clogs of amorphous aggregates of peptides were detected by TEM in line with the lower ThT fluorescence (**Figure 5.H-I**).

To explain the biphasic trend observed, a mechanism involving the independent assembly of  $Zn(A\beta_{1-40})$  and  $A\beta_{1-40}$  is proposed (**Scheme 2**, blue box). The first process (①) is rapid and corresponds to the aggregation of  $Zn(A\beta_{1-40})$ , as the ThT fluorescence intensity of the intermediate plateau depends almost linearly on the Zn:peptide ratio. The second process (②) is slower and corresponds to the formation of  $A\beta_{1-40}$  nuclei that will further recruit  $A\beta_{1-40}$  and  $Zn(A\beta_{1-40})$ , in line with the delayed apparition of  $A\beta_{1-40}$  nuclei at higher level of  $Zn(A\beta_{1-40})$ . At 1 equiv. and above, the formation of  $A\beta_{1-40}$  nuclei is too delayed to be observed in the time window of the experiment, in line with notion that most of the peptide being under its Zn-bound form in less-structured aggregates.

Similar self-assembly experiments performed with  $A\beta_{4-40}$  are shown in **Figure 5.C**. Zn induced an overall slow-down of the assembly process, that depends monotonously, almost linearly, with the Zn:peptide ratio. This is mirrored by the change in the three key kinetic parameters upon increasing the Zn:peptide ratio: increase in the  $t_{1/2} / t_{1/2}^*$  (from about 10h to 30h), decrease in the slope  $k / k^*$  (from 0.3 to 0.04 h<sup>-1</sup>) and a 6-fold decrease in the  $\Delta F / \Delta F^*$  (**Table S6**). The morphology of the fibrils was also modified by the presence of increasing Zn:peptide ratio with shorter and more amorphous aggregates compared to the one obtained with the peptide alone (**Figure 5.P-U**), consistently with the drop of fluorescence intensity. The two-step assembly process induced by Zn for  $A\beta_{1-40}$  is detected but to a much lesser extent (inset in **Figure 5.C**). Hence, a mechanism similar to that of  $A\beta_{1-40}$  is proposed, except that the various reactions are involved at different magnitudes (**Scheme 2**, green box). Formation of  $Zn(A\beta_{4-40})$  (①) is predominantly observed for Zn:peptide ratio higher than 1 while it was detected for lower Zn:peptide ratio in the case of  $A\beta_{1-40}$ . This can be explained by considering: (i) a lower propensity of  $Zn(A\beta_{4-40})$  to aggregate compared to  $Zn(A\beta_{1-40})$ , (ii) the lower affinity of Zn for  $A\beta_{4-40}$ , (iii) the resulting faster exchange between  $Zn(A\beta_{4-40})$  and  $A\beta_{4-40}$  (assuming that the association rate is similar for both peptides), and (iv) the very rapid assembly of  $A\beta_{4-40}$  (②) preventing the observation of  $Zn(A\beta_{4-40})$  aggregation. At substoichiometric Zn:peptide ratio, Zn induces the formation of less ordered fibrils compared to the corresponding apo-peptide as mirrored by a ThT intensity divided by about 2-fold at 0.5 equiv. Zn. This contrasts with  $A\beta_{1-40}$  for which regardless of the presence of Zn ( $\leq 0.5$  equiv.), the final intensity was similar (**Table S6**).

Lastly, the co-assembly of an equimolar mixture of  $A\beta_{1-40}$  and  $A\beta_{4-40}$  was studied in the presence of different ratios of Zn ions (**Figure 5.B**). As in the case of  $A\beta_{4-40}$ , the effects observed on the kinetic parameters depends monotonously on the Zn:peptide ratio (**Table 2** and **S6**) up to 0.5 equiv. of Zn. At 0.1 and 0.2 equiv. of Zn, the  $t_{1/2} / t_{1/2}^*$  was increased (from approx. 10h to 18h) while  $k / k^*$  was lower (from 0.48 to 0.21 h<sup>-1</sup>). At 0.5 equiv. of Zn, a two-step process was observed reminiscent of the trend observed for  $A\beta_{1-40}$  but to a lesser extent. At 1.0 equiv. of Zn(II) as directly compared in **Figure 4.B**, a



result similar to the one detected in the case of  $A\beta_{1-40}$  was observed with a rapid increase of the ThT fluorescence in the very first hours of the experiment, while the decrease of the maximal ThT fluorescence intensity was closer to the one observed in the case of  $A\beta_{4-40}$  (4-times decrease for the mixture of peptides versus about 5-times for  $A\beta_{4-40}$  and 1.2 for  $A\beta_{1-40}$ , **Table 1**). The morphology of the aggregates revealed that, as for the peptides taken independently, Zn addition induced more amorphous species (**Figure 5.J-O**). The effect was observed from 0.5 equiv. of Zn as in the case of  $A\beta_{4-40}$  and in contrast to the case of  $A\beta_{1-40}$ , for which amorphous species were detected from 1.0 equiv. of Zn. The effects of Zn on  $A\beta_{1-40}$  and  $A\beta_{4-40}$  co-assembly are proposed in **Scheme 2** (black box) and compared to those of  $A\beta_{1-40}$  and  $A\beta_{4-40}$  self-assembly (blue and green boxes, respectively). At low Zn:peptide ratio (0.1 to 0.2 equiv.), the proposed mechanism relies on the formation of  $Zn(A\beta_{1-40})$  in presence of apo- $A\beta_{4-40}$ , in line with the respective affinity of both peptides for Zn. This is followed by the formation of  $A\beta_{4-40}$  nuclei and/or  $A\beta_{1-40}/A\beta_{4-40}$  heteronuclei, consistent with the faster nucleation of  $A\beta_{4-40}$  versus  $A\beta_{1-40}$ . Finally, the nuclei produced recruit apo- $A\beta_{1/4-40}$  and  $Zn(A\beta_{1-40})$  to form Zn-containing  $A\beta_{4-40}$ -like hetero-fibrils. Pathway **2** is predominant over **1** that corresponds to the formation of  $Zn(A\beta_{1-40})$  aggregates. This is indicated by: (i) the very low ThT fluorescence increase observed during the first hours of the co-assembly process that equals about half of the intensity of the corresponding plateau in the  $A\beta_{1-40}$  self-assembly experiments (compare insets in **Figure 5.A** and **B**), (ii) the sigmoidal ThT rise that is weakly slowed-down compared to the one observed in absence of Zn (increase of  $t^*_{1/2}$  by about 1.5 to 2-fold, and decrease in  $k^*$  by about 2-fold, **Table 2**), and (iii) the formation of mainly fibrillar assemblies as evidence by TEM pictures (**Figure 5-K,L**). At 0.5 equiv. of Zn, Zn is bound to both peptides, although preferentially to  $A\beta_{1-40}$  in line with the respective affinities of Zn for both peptides. In this case (compared to 0.1 and 0.2 equiv. Zn), pathway **1** contributes more although pathway **2** is still present. Formation of  $Zn(A\beta_{1-40})$  aggregates coexist with the formation of  $A\beta_{4-40}$  nuclei that recruit both apo- and Zn-bound  $A\beta_{1/4-40}$ , eventually forming less-structured fibrils. This is shown by (i) a second sigmoidal process that is more significantly delayed with an increased  $t^*_{1/2}$  and decreased  $k^*$  (**Table 2**) and (ii) TEM pictures that show mainly ill-structured aggregates, in line with lower ThT intensity (**Figure 5.M**). At 1.0 equiv. of Zn and above, both peptides are metalated and only the formation of  $Zn(A\beta_{1/4-40})$  aggregates (pathway **1**) is observed in agreement with the lower ThT intensity and ill-defined aggregates observed by TEM (**Figure 5.N,O**). The kinetic curves of the co-assembly do not show any sigmoidal feature, just a steep increase whose ThT fluorescence intensity is about the average between the curves of  $Zn(A\beta_{1-40})$  and  $Zn(A\beta_{4-40})$  (**Figure 4.B**).

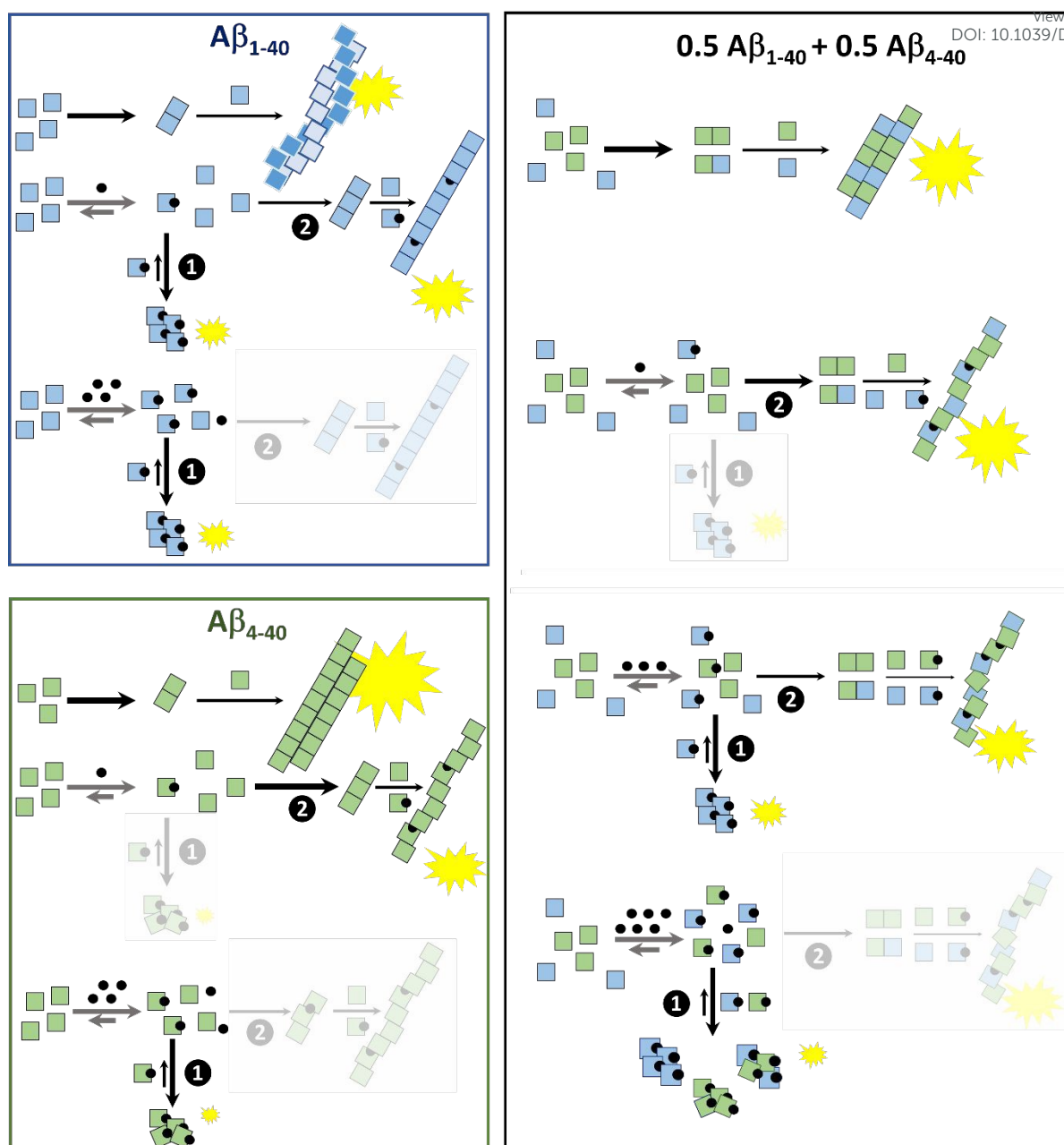
**Table 2.** Kinetic parameters of the  $A\beta_{1-40}$ ,  $A\beta_{4-40}$  and  $A\beta_{1-40}+A\beta_{4-40}$  assembly process in presence of Zn. N.D.: not determined. See Experimental Section for details on how the parameters were evaluated.

Zinc added (equiv.)	$t_{1/2}$ (h)			$k$ (h <sup>-1</sup> )		
	$A\beta_{1-40}$ ( $t_{1/2}$ )	$A\beta_{1-40}+A\beta_{4-40}$	$A\beta_{4-40}$	$A\beta_{1-40}$	$A\beta_{1-40}+A\beta_{4-40}$	$A\beta_{4-40}$
0	40.7 ± 2.4	11.1 ± 0.4	9.5 ± 0.1	0.295 ± 0.054	0.479 ± 0.131	0.333 ± 0.001
0.1	50.4 ± 12.3 <sup>[a]</sup>	13.4 ± 1.4	11.5 ± 0.4	0.244 ± 0.020 <sup>[a]</sup>	0.353 ± 0.119	0.217 ± 0.028
0.2	74.8 ± 11.9 <sup>[a]</sup>	18.2 ± 0.9 <sup>[a]</sup>	13.9 ± 1.4 <sup>[a]</sup>	0.122 ± 0.041 <sup>[a]</sup>	0.213 ± 0.019 <sup>[a]</sup>	0.218 ± 0.004 <sup>[a]</sup>
0.5	82.0 ± 10.6 <sup>[a]</sup>	58.2 ± 15.1 <sup>[a]</sup>	20.0 ± 3.0 <sup>[a]</sup>	0.023 ± 0.003 <sup>[a]</sup>	0.059 ± 0.019 <sup>[a]</sup>	0.136 ± 0.040 <sup>[a]</sup>
1.0	N.D.	N.D.	34.1 ± 7.2 <sup>[a]</sup>	N.D.	N.D.	0.041 ± 0.013 <sup>[a]</sup>

<sup>[a]</sup> the parameters are  $t^*_{1/2}$  and  $k^*$  that correspond to the second sigmoidal process.







**Scheme 2.** Proposed mechanisms of Zn-modulated self-assembly of  $A\beta_{1-40}$  (blue box) and  $A\beta_{4-40}$  (green box) and their co-assembly (black box). For a matter of simplicity, only first nucleation and elongation processes are shown. Grey arrows correspond to coordination reactions. The amounts of Zn bound to the peptides are qualitative. Width of the black arrows reflects the speed of the reaction (bolder = faster); Length of the arrows (grey of black) corresponds to the equilibrium at play (longer = thermodynamically favoured); blue square =  $A\beta_{1-40}$ , green square =  $A\beta_{4-40}$ , black circle = Zn ion, **1** corresponds to the formation of Zn:peptide aggregates and **2** to the formation of fibrillar species. Reactions that are masked correspond to a minor pathway. The amounts of black circles are proportional to the amount of Zn. Size of the yellow stars mirrors the fluorescence intensity of the ThT.



## Concluding remarks

View Article Online  
DOI: 10.1039/D5QI00850F

The proposed coordination of Zn to  $A\beta_{4-16}$  near neutral pH is given in **Scheme 1**, where it is compared to that of  $A\beta_{1-16}$  previously deduced from similar investigations.<sup>92, 93</sup> A main difference is that at pH 7.4, only a main species is present in case of  $Zn(A\beta_{1-16})$  while two species co-exist in case of  $Zn(A\beta_{4-16})$ , which differ for the participation of the N-terminal amino group in Zn binding. In addition, and more importantly, a four-fold lower Zn affinity was measured in the case of  $A\beta_{4-16}$ -CONH<sub>2</sub> relative to  $A\beta_{1-16}$ -CONH<sub>2</sub> in similar experimental conditions as those used for the assembly experiments. In a recent report, Zn affinity constants were evaluated for  $A\beta_{4-16}$ -COOH and  $A\beta_{1-16}$ -COOH, which are in the same order of magnitude as those found here ( $10^5 \text{ M}^{-1}$ ). No significant difference was found for  $A\beta_{4-16}$ -COOH and  $A\beta_{1-16}$ -COOH, in contrast to our study. Experimental conditions were different from those used here since the competitor used was Zincon at a 2:1 ratio, pH was 7.4 and NaCl concentration was 150 mM. In addition, the fitting curves were not shown, making it difficult to elaborate on the origin of these discrepancies between the two studies.<sup>121</sup>

The self-assembly of  $A\beta_{1-40}$  and  $A\beta_{4-40}$  is deeply influenced by the presence of Zn, in a concentration-dependent manner, as thoroughly described above and depicted in **Scheme 2**. Zn-induced the formation of Zn-containing fibrils at low Zn:peptide ratio and of more amorphous Zn(peptide) aggregates at higher ratio, that can co-exist with fibrils upon to 1 equiv. of Zn for  $A\beta_{1-40}$  and 0.5 equiv. of Zn for  $A\beta_{4-40}$ . The two peptides respond in a similar way but to a different extent to the Zn stimulus due to the combination of different factors, mainly a lower Zn-affinity for  $A\beta_{4-40}$  and faster self-assembly of apo- $A\beta_{4-40}$  versus apo- $A\beta_{1-40}$ .

The co-assembly of apo- $A\beta_{1-40}$  and apo- $A\beta_{4-40}$  follows a kinetic that is *in-between* those observed for  $A\beta_{4-40}$  and  $A\beta_{1-40}$  alone. Specifically, the two peptides are proposed to contribute to the elongation of  $A\beta_{4-40}$  nuclei and/or heteronuclei leading to the formation of eventual hetero-fibrils. This co-assembly was expected based on similar C-terminal sequences of both peptides as reported for  $A\beta_{11-40/42}$  and  $A\beta_{1-40/42}$ ,<sup>34</sup> and for  $A\beta_{5-42}$  and  $A\beta_{1-42}$ .<sup>122</sup> This behaviour contrasts with that reported for different C-terminal sequences (e.g.  $A\beta_{1-40}$  and  $A\beta_{1-42}$ ,<sup>33</sup>  $A\beta_{1-42}$  and  $A\beta_{11-40}$  and  $A\beta_{1-40}$  and  $A\beta_{11-42}$ <sup>34</sup>) the co-assembly of which results in the formation of homofibrils.

In the case of the Zn-modulated co-assembly, a process that involves a concerted participation of both peptides is observed as was for the apo-peptides. At low Zn:peptide ratio, the co-assembly profile resembles more that of  $A\beta_{4-40}$  self-assembly, while at higher Zn:peptide ratio (>0.5), the profile is more reminiscent of  $A\beta_{1-40}$  self-assembly. Hence the driving peptide of the co-assembly progressively changes from  $A\beta_{4-40}$  to  $A\beta_{1-40}$ . Overall, a common feature of both self- and co-assembly processes in the presence of Zn, is that a higher formation of non-fibrillar aggregates is observed at increasing Zn concentration.

While writing this paper, a study on Zn impact on  $A\beta_{4-42}$  assembly versus  $A\beta_{1-42}$  was reported.<sup>121</sup> These results are barely comparable to ours since (i) the experimental conditions (peptide concentration, stirring...) were different, (ii)  $A\beta_{1-40}$  and  $A\beta_{1-42}$  have different self-assembly properties,<sup>33, 34, 123</sup> (iii) more importantly, there is neither a complete Zn:peptide ratio dependent study nor co-assembly study but instead (cross)-seeding experiments with  $A\beta_{1-42}$ . However, one shared and thus robust trend is the higher propensity of  $A\beta_{4-40/42}$  versus  $A\beta_{1-40/42}$  to form ill-structured aggregates in presence of Zn, as characterized by TEM in both studies.

The effect of Zn on  $A\beta_{4-40}$  versus  $A\beta_{1-40}$  self-assembly is peptide-dependent as was that of Cu.<sup>57</sup> In the case of Cu, it was linked to its binding by the N-terminal ATCUN motif of  $A\beta_{4-40}$  leading to an higher affinity than in  $A\beta_{1-40}$  ( $10^{13}$  versus  $10^{10} \text{ M}^{-1}$ ) and to a Cu buried within the three first amino-acid residues (Phe4-Arg5-His6) compared to a Cu site delocalized on the first 14 residues.<sup>87, 124</sup> In the case



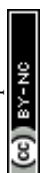
of Zn, despite similar binding sites and affinity ( $\sim 10^5 \text{ M}^{-1}$ ), a significantly distinct effect was also observed on the metal-induced modulation of  $\text{A}\beta_{1-40}$  and  $\text{A}\beta_{4-40}$  self-assembly. This indicates that, in the case of weakly bound ion such as Zn (in comparison with Cu), (i) the intrinsic apo-peptide self-assembly plays a key role since the apo-peptide is always in equilibrium with the Zn-bound peptide, (ii) more subtle coordination differences induce a significantly distinct modulatory effect, in line with the discrepancies in the reports on Zn impact on  $\text{A}\beta_{1-40/42}$  self-assembly.<sup>16, 63, 74, 77, 80-85</sup> Such metal-dependent effects are also observed for the co-assembly process.

The present study aimed to decipher how Zn modulates the co-assembly of two of the most abundant  $\text{A}\beta$  peptides detected in the brain.<sup>39-41, 43, 46, 52</sup> Going from the study of metal-induced changes in peptide self-assembly to peptides co-assembly is a necessary step forward a more biologically relevant situation and was reported only once before.<sup>57</sup> Along this line, it would be interesting to further evaluate the impact of both Cu and Zn binding on either and both peptides.<sup>125</sup> The result obtained show that for the mixture of peptides, the formation of ill-structured co-assemblies, regarded as more toxic than fibrillar ones,<sup>65, 126-128</sup> is obtained for lower Zn:peptide ratio in comparison with  $\text{A}\beta_{1-40}$  self-assembly. Otherwise stated  $\text{A}\beta_{4-40}$  modifies the Zn-modulated  $\text{A}\beta_{1-40}$  assembly in a deleterious way. This counterbalances the positive impact the  $\text{A}\beta_{4-40}$  has with respect to Cu-induced production of ROS<sup>87, 124, 129</sup> and leads to a new function of this still understudied N-terminally  $\text{A}\beta$  sequence compared to the full-length counterpart.

**Acknowledgments.** C.H. and L.d.C. acknowledge the financial support of the ANR SUPRAMY (ANR-21-CE06-0030). This work was also supported by the MITI 80PRIME program of the CNRS to N.V and C. H. (contract #256994). C.H. and E.F. acknowledge the European Synchrotron Radiation Facility (ESRF, Grenoble) for the provision of synchrotron radiation facilities under proposal numbers LS-3238 and LS-3308 and we would like to thank Dr. Olivier Proux (ESRF) and Prof. Francesco Stellato (INFN-University of Rome Tor Vergata) for assistance and support in using beamline BM16 (FAME) and XAS data analysis. We acknowledge Dr. C. Bijani (LCC-CNRS, Toulouse) for the recording of the NMR experiments and the TEM platform METi imaging facility (Toulouse). The preliminary participation of Dr. E. Atrián-Blasco in the assembly studies and the aid of Dr. L. Sabater for peptides' assembly data curation are warmly acknowledged.

## Experimental Section

**Chemicals.** HEPES and NaCl stock solutions at 500 mM were prepared by dissolving (4-(2-hydroxyethyl)piperazine-1-ethanesulfonic acid) (Thermo Fischer, USA) and NaCl (Sigma Aldrich, USA) in MilliQ Water. The pH was adjusted at pH = 7.4 by adding NaOH stock solutions. Tris stock solution at 1 mM was prepared by dissolving tris(hydroxymethyl)aminomethane (Sigma Aldrich, USA) in MilliQ Water. The pH was adjusted at pH = 12 by adding NaOH solution. Stock solutions (0.2 M) of NMR buffer  $[\text{D}_{19}]$ Bis-Tris (2,2-Bis(hydroxymethyl)-2,2',2''-nitrioltriethanol- $\text{d}_{19}$ ) or  $[\text{D}_{11}]$ Tris (Tris(hydroxymethyl- $\text{d}_3$ )amino- $\text{d}_2$ -methane) were prepared by dissolving the deuterated Bis-Tris or Tris powder (Eurisotop) in milliQ water. Peptide solutions were prepared by dissolving the peptide solid in milliQ water. NaOH solution was prepared by dissolving NaOH (Sigma Aldrich) in MilliQ Water. Thioflavin T stock solution at 1 mM was prepared by dissolving the powder (purchased from Acros Organics, USA) in MilliQ Water. The concentration was verified by absorption spectroscopy at 412 nm ( $\epsilon = 33000 \text{ M}^{-1} \cdot \text{cm}^{-1}$ ). From this stock solution, some aliquots at 250  $\mu\text{M}$  were prepared and stored in the freezer, at  $-20^\circ\text{C}$  until used. Zn(II) stock solution was prepared by dissolving  $\text{ZnSO}_4 \cdot \text{H}_2\text{O}$  (Strem Chemicals, USA) in MilliQ water. A stock solution (ca. 10 mM) of 4-(2-pyridylazo)resorcinol (PAR) was prepared by dissolving PAR monosodic salt (purchased from Acros Organics, USA) in MilliQ water.



**Peptides.**  $\text{A}\beta_{1-16}\text{-COOH}$ ,  $\text{A}\beta_{1-16}\text{-CONH}_2$  (sequences DAEFRHDSGYEVHHQK-COOH and DAEFRHDSGYEVHHQK-CONH<sub>2</sub>), and  $\text{A}\beta_{4-16}\text{-COOH}$  and  $\text{A}\beta_{4-16}\text{-CONH}_2$  (sequences FRHDSGYEVHHQK-COOH and FRHDSGYEVHHQK-CONH<sub>2</sub>) were purchased from Genecust (France) with a purity grade >95%. Solutions of these peptides were prepared at around 10 mM and kept in the fridge at 4°C until used. The concentration of the peptides was determined by UV-Visible of the Tyr10 at acidic pH ( $\epsilon_{276} - \epsilon_{296} = 1410 \text{ M}^{-1} \cdot \text{cm}^{-1}$ ) by mixing 10  $\mu\text{L}$  of the stock solution with 90  $\mu\text{L}$  of Milli-Q water.

$\text{A}\beta_{1-40}$  peptide (sequence DAEFRHDSGYEVHHQKLVFFAEDVGSNKGAIIGLMVGGVV) and  $\text{A}\beta_{4-40}$  peptide (sequence FRHDSGYEVHHQKLVFFAEDVGSNKGAIIGLMVGGVV) were also purchased from Genecust with a purity grade >95%. Peptides (around 2-3 mg) were dissolved in a monomerization solution, prepared with 100 mM Tris buffer with 6 M guanidine chloride (Alfa Aesar, USA), with an adjusted pH = 10 and a final volume of 550  $\mu\text{L}$ . Then these solutions were mildly shake on a carousel, at 20 rpm, at room temperature, overnight. After centrifugation, at 10000 rpm, at room temperature, for 10 min, the peptides were purified on an FPLC Äkta basic 10 system (GE Healthcare, USA). 500  $\mu\text{L}$  of these peptides were injected on a column Superdex 75-10/300-increase using a solution of 15 mM NaOH and 150 mM NaCl as eluant with a 0.5  $\text{mL} \cdot \text{min}^{-1}$  flow rate. Peptides were detected at 293 nm corresponding to the TyrO<sup>-</sup> absorption and at 220 nm. The retention time was about 26 min for  $\text{A}\beta_{1-40}$  and 30 min for  $\text{A}\beta_{4-40}$ . All the 500  $\mu\text{L}$  fractions corresponding to the peptides were recovered and titrated by UV-Visible of the Tyr10 at basic pH ( $\epsilon_{293} - \epsilon_{360} = 2400 \text{ M}^{-1} \cdot \text{cm}^{-1}$ ) by mixing 10  $\mu\text{L}$  of the recovered fractions with 90  $\mu\text{L}$  of NaOH 500 mM. The three most concentrated fractions were then pooled and gently mixed, to obtain 1.5 mL of peptide with a concentration of approx. 200  $\mu\text{M}$ .

**XAS.** XAS data at the Zn K-edge were acquired at the BM16 beamline of the European Synchrotron Radiation Facility (ESRF - Grenoble, France). The beamline energy was calibrated using a metallic Cu foil by setting the position of the absorption edge (defined as the first maximum of the first derivative curve) to 8979 eV. In order to prevent precipitation, samples were freshly prepared by rapidly mixing ZnSO<sub>4</sub> (final concentration 1 mM) and  $\text{A}\beta$  peptides (final concentration 1.2 mM) in 100 mM HEPES buffer at pH 7.4, transferred into a sample holder (closed by two Kapton films) and immediately frozen in liquid N<sub>2</sub> before introduction in a liquid He cryostat, where the temperature was kept at 10 K throughout the measurement in order to minimize radiation damage. Spectra were recorded in fluorescence mode using a 13-element solid-state Ge detector. The software Larch<sup>130</sup> was used to normalize XANES data and extract the EXAFS.

**NMR.** <sup>1</sup>H NMR and TOCSY were recorded on a Bruker Ascend 600 spectrometer, equipped with 5 mm triple resonance inverse Z-gradient probe (TBI <sup>1</sup>H, <sup>31</sup>P, BB). Chemical shifts for <sup>1</sup>H were relative to TMS using <sup>1</sup>H (residual) chemical shifts of the solvent as secondary standard. All the spectra were acquired at 298 K using Bruker pulse program "zgsp" featuring a water-suppression sequence and the following parameters: spectral width, 12 ppm, 30° nutation angle duration, 9.5  $\mu\text{s}$  recycling delay 2-s (1-s acquisition time and 1-s relaxation delay).

The NMR samples were prepared from stock solutions to obtain a mixture with 200  $\mu\text{M}$  of  $\text{A}\beta$  peptides, 50 mM of [D<sub>19</sub>]Bis-Tris (used for pH = 6.8, 7.4, 7.6 and 7.9) or [D<sub>11</sub>]Tris (for pH = 8.2). The pH of these solutions was, then, adjusted by adding NaOH or H<sub>2</sub>SO<sub>4</sub> solutions. Zn(II) stock solution in milliQ water was directly added to the mixture in the NMR tube using a Teflon tube.

**Competition experiments to evaluate Zn(II) binding affinity.** The L<sub>2</sub> ligand (*N,N'*-Bis[(5-sulfonato-2-hydroxy)benzyl]-*N,N'*-dimethyl-ethane-1,2-diamine) was prepared as previously described. The competitions were recorded on an Agilent 8453 spectrometer with a Peltier temperature controller unit which maintained the temperature at 25°C, with a constant stirring at 800 rpm. Briefly and as described before, 60  $\mu\text{M}$  of the ligand L<sub>2</sub> and 50  $\mu\text{M}$  of Zn(II) were mixed in a UV-cell, with 50 mM



HEPES at pH = 7.1, in milliQ water. Then, 1 to 10 equiv. of A $\beta$  peptide were added (compared to the theoretical Zn concentrations). As the  $K_a$  value of the complex Zn(L<sub>2</sub>) was highly dependent of the pH, the pH of the peptides stock solutions must be adjusted to pH ~ 7 to avoid any modification of the pH during the addition of the peptides. These experiments were realised at least twice for each peptide.

The data analysis was realised following a two-step procedure to determine the  $K_a$  value of the Zn(A $\beta$ ) complexes, as previously described.<sup>115</sup>

**Step 1**, real concentrations of the ligand L<sub>2</sub> and of Zn(II) ions were determined at pH = 7.1. L<sub>2</sub> concentration was determined following its absorbance at 254 nm and using its  $\epsilon_{254} = 6130 \text{ M}^{-1} \text{ cm}^{-1}$ . Similarly, Zn(II) ions concentration was determined following the absorbance of Zn(L<sub>2</sub>) complex at 254 nm and using its  $\epsilon_{254} = 30000 \text{ M}^{-1} \text{ cm}^{-1}$ .

**Step 2**, the absorbance of the competition experiments at 254 nm was plotted as a function of the real peptide concentrations and reproduced following an in-house procedure and using the real concentrations of L<sub>2</sub> ligand and Zn(II) ions as starting parameters (determined in step 1).

Absorbance was calculated according to:

$$Abs = ([A\beta] - [\alpha])\epsilon_{254 \text{ nm}}^{A\beta} + ([Zn] - [\alpha])\epsilon_{254 \text{ nm}}^{L_2-Zn} + [\alpha]\epsilon_{254 \text{ nm}}^{A\beta-Zn} + ([L_2] - [Zn] + [\alpha])\epsilon_{254 \text{ nm}}^{L_2}$$

where  $\alpha$  stands for the progression of the reaction: A $\beta$  + Zn(II)  $\rightarrow$  A $\beta$ -Zn(II)

As Zn(II) should be coordinated by A $\beta$  peptides or by the ligand L<sub>2</sub>, it was hypothesised that there is no free Zn(II) ions in solution.

$$\frac{K_d^{A\beta-Zn}}{K_d^{L_2-Zn}} = \frac{[A\beta][Zn]}{[\alpha]} \cdot \frac{[L_2Zn]}{[L_2][Zn]}, \text{ with the starting concentrations: } \frac{K_d^{A\beta-Zn}}{K_d^{L_2-Zn}} = \frac{[A\beta]_0 - [\alpha]}{[\alpha]} \cdot \frac{[Zn]_0 - [\alpha]}{[L_2]_0 - [Zn]_0 + [\alpha]}$$

This gives a quadratic equation:  $a\alpha^2 + b\alpha + c = 0$  where  $\alpha = \frac{-b + \sqrt{\Delta}}{2a}$  with  $\Delta = b^2 - 4ac$ ,

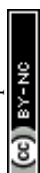
$$a = \frac{K_d^{A\beta-Zn}}{K_d^{L_2-Zn}} - 1, b = \frac{K_d^{A\beta-Zn}}{K_d^{L_2-Zn}}([L_2] - [Zn]) + ([A\beta] + [Zn]) \text{ and } c = -[A\beta][Zn].$$

$K_d^{A\beta-Zn}$  value was adjusted to obtain the best reproduction possible of the experimental data.

The possibility of that a ternary species contributes to the decrease of the absorbance at 254 nm upon addition of the peptides was ruled out based on the facts that the UV-Vis spectrum of the Zn(L<sub>2</sub>) complex was not modified by the addition of high excess of either of Imidazole, mimicking the His side chains of the A $\beta$  peptide, or of glycine, mimicking the Asp and Glu side chains (**Figure S8**).

**Potentiometric titrations** were performed on a Titrand 907 automatic titrator (Metrohm) using a combined glass Ag/AgCl electrode (InLabMicro, Mettler Toledo). The electrode was calibrated by titrating nitric acid. The CO<sub>2</sub>-free solution of 0.1 M NaOH was used as the titrant. All experiments were performed under argon, at 25°C. Sample volumes were 1.5 mL. The samples contained 0.5 mM A $\beta_{1-16}$ -CONH<sub>2</sub> or A $\beta_{4-16}$ -CONH<sub>2</sub> peptides dissolved in 8 mM HNO<sub>3</sub>/92 mM KNO<sub>3</sub>.

**Kinetic monitoring of A $\beta$  assembly.** Assembly kinetics were realised by following the Thioflavin T (noted ThT) fluorescence. The kinetics were recorded on a fluorimeter plate reader FLUOStar Omega (BMG Labtech, Germany) by exciting the ThT at 440 nm and following its emission at 490 nm using the corresponding filters. The gain was set up at 1400. The kinetics were realised at 37°C, with a stirring at 200 rpm, double orbital for 15 s before each measurement, and the fluorescence emission was measured every 300 s. The experiments were realised in Greiner BioOne 384-wells plates low retention (Dutscher, France) by mixing the appropriate concentrations of each reactant (100 mM HEPES at pH = 7.4 (measured at 20°C), 100mM NaCl (except for the data reported in the full text), 10  $\mu$ M ThT, different concentrations of Zn(II) from a stock solution at 10 mM). The total concentration of the peptide was kept at 20  $\mu$ M in the wells. Ethylenediaminetetraacetic acid (EDTA) at 0.02  $\mu$ M was added





to chelate possible traces of metallic contaminants as EDTA complexes have no significant impact on A $\beta$  self-assemblies. Each condition was run in at least quadruplicate and six independent experiments were realised.

**Evaluation of kinetic parameters of A $\beta$  assembly.** The ThT fluorescence increase can be considered, in general, as a sigmoidal curve described by the equation:

$$F(t) = F_0 + \frac{F_{max} - F_0}{1 + e^{-k(t - t_{1/2})}} = F_0 + \frac{\Delta F}{1 + e^{-k(t - t_{1/2})}}$$

where  $F_0$  is the initial ThT fluorescence value,  $\Delta F$  is the ThT fluorescence increase ( $F_{max} - F_0$ ),  $k$  is the growth rate, and  $t_{1/2}$  is the time at which the ThT fluorescence increase equals half of its maximal value ( $F_0 + \frac{F_{max} - F_0}{2}$ ).

Several experimental curves cannot be appropriately fitted according to this equation, since for instance, a lack of symmetry was observed in A $\beta_{4-40}$  kinetic curves and the Zn-modified A $\beta$  assemblies exhibit a biphasic ThT rise. Hence to compare all curves, a custom routine was developed to evaluate the key parameters. The parameters are noted as  $t^*_{1/2}$ ,  $k^*$  and  $\Delta F^*$  when a second and sigmoidal process occurs (**Scheme S5**). The total amount of fibrillar species was assumed to remain constant up to 0.5 equiv. of Zn, corresponding ThT curves were then first normalized.

The inflexion point,  $t_{1/2}$  or  $t^*_{1/2}$  was determined as the time at which  $F(t) = F_0 + \frac{\Delta F}{2}$  (or  $F(t) = F_1 + \frac{\Delta F^*}{2}$  where  $F_1$  is the value of the ThT Fluorescence after the first detectable Zn-induced non-sigmoidal process).

An apparent growth rate, later noted for matter of simplicity  $k$  was estimated by calculating the slope at  $t = t_{1/2}$  as  $k = 4 \left( \frac{F_{60\%} - F_{40\%}}{t_{60\%} - t_{40\%}} \right)$ , where  $F_{60\%}$  and  $F_{40\%}$  equals 60% and 40% of the maximal ThT fluorescence increase, respectively, and  $t_{60\%}$  and  $t_{40\%}$  are the times at which these fluorescence values occur. The  $\frac{1}{4}$  factor arises from the fact that the slope at the inflection point ( $t = t_{1/2}$ ) for a sigmoid equation  $S(t) = \frac{1}{1 + e^{-k(t - t_{1/2})}}$  is equal to  $S'(t_{1/2}) = \frac{k}{4}$ . Similar equations apply for  $k^*$  using  $t^*_{1/2}$  and  $\Delta F^*$  (**Scheme S5**).

**Transmission Electronic Microscopy.** The tested samples were recovered after 7 days of aggregation at 37°C in a 384-wells plate. Each sextuplicate was pooled in low-binding microtubes. The samples were prepared for electron microscopy following the classical negative procedure: a 10  $\mu$ L aliquot of the sample solution was incubated for 1 min on Formvar-carbon-coated grids (purchased from Electron Microscopy Sciences, USA) and then, dried and negatively stained using 1% uranyl acetate for 1 min. The obtained grids were observed with TEM microscope (Jeol JEM 1400, JEOL Inc, USA) at 80 kV. The pictures were acquired using a digital camera (Gatan Orius, Gatan Inc, USA) at 3000, 4000, 6000 and 12000 magnifications.

## Zn(II) quantification in supernatants and fibrils

In order to separate the supernatant from the fibrils, microplates were centrifuged at 3000 rpm for 1h at r.t. 90  $\mu$ L of supernatant were then taken from each well and mixed with 10  $\mu$ L of PAR 1 mM (final concentration 100  $\mu$ M). To achieve complete recovery of Zn from the fibrils, the residual pellets were resuspended in each well with 90  $\mu$ L of PAR 100  $\mu$ M in HEPES 100 mM, EDTA 0.02  $\mu$ M at pH ca. 3. The microplate was shaken at 500 rpm for 1h at r.t. Then, the resuspended solutions were taken and their pH was adjusted to ca. 7.4. The absorption spectra of both supernatants and resuspended pellets were





recorded in a microplate (Greiner BioOne 384-wells plates low retention) using a ClarioStar microplate reader (BMG Labtech). The absorbance of  $\text{Zn}(\text{PAR})_2$  at 490 nm<sup>119</sup> was used to estimate the concentration of Zn based on a calibration curve obtained with PAR 100  $\mu\text{M}$  in HEPES 100 mM, EDTA 0.02  $\mu\text{M}$  at pH 7.4 and Zn concentrations spanning from 2  $\mu\text{M}$  to 40  $\mu\text{M}$ .

View Article Online  
DOI: 10.1039/D5QI00850F



## References.

View Article Online  
DOI: 10.1039/D5QI00850F

1. S. Gauthier, P. Rosa-Neto, J. A. Morais and C. Webster, *World Alzheimer Report 2021 : Journey through the diagnosis of dementia*, Alzheimer's Disease International, 2021.
2. A. Wimo, G.-C. Ali, M. Guerchet, M. Prince, M. Prina and Y.-T. Wu, *World Alzheimer Report 2015 : The Global Impact of Dementia : An analysis of prevalence, incidence, cost and trends*, Alzheimer's Disease International, 2015.
3. World Health Organisation, Dementia, <https://www.who.int/news-room/fact-sheets/detail/dementia>).
4. J. A. Hardy and G. A. Higgins, Alzheimer's Disease: The Amyloid Cascade Hypothesis, *Science*, 1992, **256**, 184-185.
5. D. J. Selkoe and J. Hardy, The amyloid hypothesis of Alzheimer's disease at 25 years, *EMBO molecular medicine*, 2016, **8**, 595-608.
6. G. B. Frisoni, D. Altomare, D. R. Thal, F. Ribaldi, R. van der Kant, R. Ossenkoppele, K. Blennow, J. Cummings, C. van Duijn, P. M. Nilsson, P.-Y. Dietrich, P. Scheltens and B. Dubois, The probabilistic model of Alzheimer disease: the amyloid hypothesis revised, *Nat. Rev. Neurosci.*, 2022, **23**, 53-66.
7. S. McGirr, C. Venegas and A. Swaminathan, Alzheimer's Disease: A Brief Review. , *J. Exp. Neurol.*, 2020, **1**, 89-98.
8. M. A. Lovell, J. D. Robertson, W. J. Teesdale, J. L. Campbell and W. R. Markesbery, Copper, iron and zinc in Alzheimer's disease senile plaques, *J. Neurol. Sci.*, 1998, **158**, 47-52.
9. L. M. Miller, Q. Wang, T. P. Telivala, R. J. Smith, A. Lanzirotti and J. Miklossy, Synchrotron-based infrared and X-ray imaging shows focalized accumulation of Cu and Zn co-localized with  $\beta$ -amyloid deposits in Alzheimer's disease, *J. Struct. Biol.*, 2006, **155**, 30-37.
10. M. Chourrout, C. Sandt, T. Weitkamp, T. Dučić, D. Meyronet, T. Baron, J. Klohs, N. Rama, H. Boutin, S. Singh, C. Olivier, M. Wiart, E. Brun, S. Bohic and F. Chauveau, Virtual histology of Alzheimer's disease: Biometal entrapment within amyloid- $\beta$  plaques allows for detection via X-ray phase-contrast imaging, *Acta Biomaterialia*, 2023, **170**, 260-272.
11. J. Everett, J. Brooks, V. Tjendana Tjhin, F. Lermyte, I. Hands-Portman, G. Plascencia-Villa, G. Perry, P. J. Sadler, P. B. O'Connor, J. F. Collingwood and N. D. Telling, Label-Free In Situ Chemical Characterization of Amyloid Plaques in Human Brain Tissues, *ACS Chemical Neuroscience*, 2024, **15**, 1469-1483.
12. F. Scollo and C. La Rosa, Amyloidogenic Intrinsically Disordered Proteins: New Insights into Their Self-Assembly and Their Interaction with Membranes, *Life*, 2020, **10**, 144.
13. P. Faller and C. Hureau, Bioinorganic chemistry of copper and zinc ions coordinated to amyloid- $\beta$  peptide, *Dalton Trans.*, 2009, DOI: 10.1039/B813398K, 1080-1094.
14. C. Hureau, Coordination of redox active metal ions to the amyloid precursor protein and to amyloid- $\beta$  peptides involved in Alzheimer disease. Part 1: An overview, *Coord. Chem. Rev.*, 2012, **256**, 2164-2174.
15. A. Abelein, Metal Binding of Alzheimer's Amyloid- $\beta$  and Its Effect on Peptide Self-Assembly, *Accounts of Chemical Research*, 2023, **56**, 2653-2663.
16. E. Atrian-Blasco, P. Gonzalez, A. Santoro, B. Alies, P. Faller and C. Hureau, Cu and Zn coordination to amyloid peptides: From fascinating chemistry to debated pathological relevance, *Coord. Chem. Rev.*, 2018, **375**, 38-55.
17. M. S. Dutta and S. Basu, Identifying the key residues instrumental in imparting stability to amyloid beta protofibrils – a comparative study using MD simulations of 17–42 residues, *Journal of Biomolecular Structure and Dynamics*, 2021, **39**, 431-456.
18. K. Röder and D. J. Wales, Energy Landscapes for the Aggregation of A $\beta$ 17–42, *JACS*, 2018, **140**, 4018-4027.



19. D. Im, S. Kim, G. Yoon, D. G. Hyun, Y.-G. Eom, Y. E. Lee, C. H. Sohn, J.-M. Choi and H. I. Kim, Decoding the Roles of Amyloid- $\beta$  (1–42)'s Key Oligomerization Domains toward Designing Epitope-Specific Aggregation Inhibitors, *JACS Au*, 2023, **3**, 1065-1075.
20. M. Sunde and C. Blake, in *Advances in Protein Chemistry*, eds. F. M. Richards, D. S. Eisenberg and P. S. Kim, Academic Press, 1997, vol. 50, pp. 123-159.
21. B. Holcombe, A. Foes, S. Banerjee, K. Yeh, S.-H. J. Wang, R. Bhargava and A. Ghosh, Intermediate Antiparallel  $\beta$  Structure in Amyloid  $\beta$  Plaques Revealed by Infrared Spectroscopic Imaging, *ACS Chemical Neuroscience*, 2023, **14**, 3794-3803.
22. Y. Yang, D. Arseni, W. Zhang, M. Huang, S. Lövestam, M. Schweighauser, A. Kotecha, A. G. Murzin, S. Y. Peak-Chew, J. Macdonald, I. Lavenir, H. J. Garringer, E. Gelpi, K. L. Newell, G. G. Kovacs, R. Vidal, B. Ghetti, B. Ryskeldi-Falcon, S. H. W. Scheres and M. Goedert, Cryo-EM structures of amyloid- $\beta$  42 filaments from human brains, *Science*, 2022, **375**, 167-172.
23. M. Törnquist, T. C. T. Michaels, K. Sanagavarapu, X. Yang, G. Meisl, S. I. A. Cohen, T. P. J. Knowles and S. Linse, Secondary nucleation in amyloid formation, *Chem. Commun.*, 2018, **54**, 8667-8684.
24. S. Linse, Monomer-dependent secondary nucleation in amyloid formation, *Biophys Rev*, 2017, **9**, 329-338.
25. G. Meisl, J. B. Kirkegaard, P. Arosio, T. C. T. Michaels, M. Vendruscolo, C. M. Dobson, S. Linse and T. P. J. Knowles, Molecular mechanisms of protein aggregation from global fitting of kinetic models, *Nature Protocols*, 2016, **11**, 252-272.
26. Z. L. Almeida and R. M. M. Brito, Structure and Aggregation Mechanisms in Amyloids, *Molecules*, 2020, **25**.
27. T. C. T. Michaels, D. Qian, A. Šarić, M. Vendruscolo, S. Linse and T. P. J. Knowles, Amyloid formation as a protein phase transition, *Nat. Rev. Phys.*, 2023, **5**, 379-397.
28. R. Wetzel, Kinetics and Thermodynamics of Amyloid Fibril Assembly, *Accounts of Chemical Research*, 2006, **39**, 671-679.
29. A. K. Buell, The growth of amyloid fibrils: rates and mechanisms, *Biochem. J.*, 2019, **476**, 2677-2703.
30. E. Chatani and N. Yamamoto, Recent progress on understanding the mechanisms of amyloid nucleation, *Biophysical Reviews*, 2018, **10**, 527-534.
31. S. Jalali, R. Zhang, M. P. Haataja and C. L. Dias, Nucleation and Growth of Amyloid Fibrils, *The Journal of Physical Chemistry B*, 2023, **127**, 9759-9770.
32. S. Hadi Alijanvand, A. Peduzzo and A. K. Buell, Secondary Nucleation and the Conservation of Structural Characteristics of Amyloid Fibril Strains, *Frontiers in Molecular Biosciences*, 2021, **8**, 669994.
33. R. Cukalevski, X. Yang, G. Meisl, U. Weininger, K. Bernfur, B. Frohm, T. P. J. Knowles and S. Linse, The A $\beta$ 40 and A $\beta$ 42 peptides self-assemble into separate homomolecular fibrils in binary mixtures but cross-react during primary nucleation, *Chem. Sci.*, 2015, **6**, 4215-4233.
34. J. D. Barritt, N. D. Younan and J. H. Viles, N-Terminally Truncated Amyloid- $\beta$ (11–40/42) Cofibrillizes with its Full-Length Counterpart: Implications for Alzheimer's Disease, *Angew. Chem. Int. Ed.*, 2017, **56**, 9816-9819.
35. F. Abedin and S. A. Tatulian, Mutual structural effects of unmodified and pyroglutamylated amyloid  $\beta$  peptides during aggregation, *Journal of Peptide Science*, 2021, **n/a**, e3312.
36. M. O. Quartey, J. N. K. Nyarko, J. M. Maley, J. R. Barnes, M. A. C. Bolanos, R. M. Heistad, K. J. Knudsen, P. R. Pennington, J. Buttigieg, C. E. De Carvalho, S. C. Leary, M. P. Parsons and D. D. Mousseau, The A $\beta$ (1–38) peptide is a negative regulator of the A $\beta$ (1–42) peptide implicated in Alzheimer disease progression, *Sci. Rep.*, 2021, **11**, 431.
37. R. J. Brien and P. C. Wong, Amyloid Precursor Protein Processing and Alzheimer's Disease, *Annual Review of Neuroscience*, 2011, **34**, 185-204.



38. Y.-w. Zhang, R. Thompson, H. Zhang and H. Xu, APP processing in Alzheimer's disease, *Molecular Brain*, 2011, **4**, 3. Article Online  
DOI: 10.1039/D5QI00850F
39. D. M. Holtzman, J. C. Morris and A. M. Goate, Alzheimer's disease: the challenge of the second century., *Sci. Transl. Med.*, 2011, **3**, 77sr71.
40. A. Dorey, A. Perret-Liaudet, Y. Tholance, A. Fourier and I. Quadrio, Cerebrospinal Fluid A $\beta$ 40 Improves the Interpretation of A $\beta$ 42 Concentration for Diagnosing Alzheimer's Disease., *Front. Neurol.*, 2015, **6**.
41. E. Portelius, A. Westman-Brinkmalm, H. Zetterberg and K. Blennow, Determination of  $\beta$ -Amyloid Peptide Signatures in Cerebrospinal Fluid Using Immunoprecipitation-Mass Spectrometry, *Journal of Proteome Research*, 2006, **5**, 1010-1016.
42. E. Portelius, A. J. Tran, U. Andreasson, R. Persson, G. Brinkmalm, H. Zetterberg, K. Blennow and A. Westman-Brinkmalm, Characterization of Amyloid  $\beta$  Peptides in Cerebrospinal Fluid by an Automated Immunoprecipitation Procedure Followed by Mass Spectrometry, *J. Proteome Res.*, 2007, **6**, 4433-4439.
43. E. Portelius, N. Bogdanovic, M. K. Gustavsson, I. Volkmann, G. Brinkmalm, H. Zetterberg, B. Winblad and K. Blennow, Mass spectrometric characterization of brain amyloid beta isoform signatures in familial and sporadic Alzheimer's disease, *Acta Neuropathol. (Berl)*. 2010, **120**, 185-193.
44. M. P. Kummer and M. T. Heneka, Truncated and modified amyloid-beta species, *Alzheimer's res. ther.*, 2014, **6**, 28.
45. N. C. Wildburger, T. J. Esparza, R. D. LeDuc, R. T. Fellers, P. M. Thomas, N. J. Cairns, N. L. Kelleher, R. J. Bateman and D. L. Brody, Diversity of Amyloid-beta Proteoforms in the Alzheimer's Disease Brain, *Sci. Rep.*, 2017, **7**, 9520.
46. O. Wirths, Zampar, S. & Weggen, S. in 107–122 (2019). doi:10.15586/alzheimersdisease.2019.ch7, *N-Terminally Truncated A $\beta$  Peptide Variants in Alzheimer's Disease.*, 2019.
47. C. L. Masters, G. Multhaup, G. Simms, J. Pottgiesser, R. N. Martins and K. Beyreuther, Neuronal origin of a cerebral amyloid: neurofibrillary tangles of Alzheimer's disease contain the same protein as the amyloid of plaque cores and blood vessels, *EMBO J.*, 1985, **4**, 2757-2763-2763.
48. C. L. Masters, G. Simms, N. A. Weinman, G. Multhaup, B. L. McDonald and K. Beyreuther, Amyloid plaque core protein in Alzheimer disease and Down syndrome, *Proc. Natl. Acad. Sci. U.S.A.*, 1985, **82**, 4245-4249.
49. Y. Bouter, K. Dietrich, J. L. Wittnam, N. Rezaei-Ghaleh, T. Pillot, S. Papot-Couturier, T. Lefebvre, F. Sprenger, O. Wirths, M. Zweckstetter and T. A. Bayer, N-truncated amyloid  $\beta$  (A $\beta$ ) 4-42 forms stable aggregates and induces acute and long-lasting behavioral deficits, *Acta Neuropathol.*, 2013, **126**, 189-205.
50. H. Lewis, D. Beher, N. Cookson, A. Oakley, M. Piggott, C. M. Morris, E. Jaros, R. Perry, P. Ince, R. A. Kenny, C. G. Ballard, M. S. Shearman and R. N. Kalaria, Quantification of Alzheimer pathology in ageing and dementia: age-related accumulation of amyloid- $\beta$ (42) peptide in vascular dementia, *Neuropathology and Applied Neurobiology*, 2006, **32**, 103-118.
51. O. Wirths, S. Walter, I. Kraus, H. W. Klafki, M. Stazi, T. J. Oberstein, J. Ghiso, J. Wiltfang, T. A. Bayer and S. Weggen, N-truncated A $\beta$ 4-x peptides in sporadic Alzheimer's disease cases and transgenic Alzheimer mouse models, *Alzheimer's res. ther.*, 2017, **9**, 80.
52. E. Portelius, T. Lashley, A. Westerlund, R. Persson, N. C. Fox, K. Blennow, T. Revesz and H. Zetterberg, Brain Amyloid-Beta Fragment Signatures in Pathological Ageing and Alzheimer's Disease by Hybrid Immunoprecipitation Mass Spectrometry, *J. Neurodegener. Dis.*, 2015, **15**, 50-57.
53. L. Morelli, R. E. Llovera, I. Mathov, L.-F. Lue, B. Frangione, J. Ghiso and E. M. Castaño, Insulin-degrading Enzyme in Brain Microvessels: PROTEOLYSIS OF AMYLOID  $\beta$  VASCULOTROPIC VARIANTS AND REDUCED ACTIVITY IN CEREBRAL AMYLOID ANGIOPATHY\*, *J. Biol. Chem.*, 2004, **279**, 56004-56013.
54. G. Grasso, A. Pietropaolo, G. Spoto, G. Pappalardo, G. R. Tundo, C. Ciaccio, M. Coletta and E. Rizzarelli, Copper(I) and Copper(II) Inhibit A $\beta$  Peptides Proteolysis by Insulin-Degrading Enzyme Differently: Implications for Metallostasis Alteration in Alzheimer's Disease, *Chem. Eur. J.*, 2011, **17**, 2752-2762.



55. S. Howell, J. Nalbantoglu and P. Crine, Neutral endopeptidase can hydrolyze  $\beta$ -amyloid(1–40) but shows no effect on  $\beta$ -amyloid precursor protein metabolism, *Peptides*, 1995, **16**, 647-652. DOI: 10.1039/D5QI00850F
56. H. Kanemitsu, T. Tomiyama and H. Mori, Human neprilysin is capable of degrading amyloid  $\beta$  peptide not only in the monomeric form but also the pathological oligomeric form, *Neuroscience Letters*, 2003, **350**, 113-116.
57. E. Stefaniak, E. Atrian-Blasco, W. Goch, L. Sabater, C. Hureau and W. Bal, The Aggregation Pattern of A $\beta$ 1–40 is Altered by the Presence of N-Truncated A $\beta$ 4–40 and/or Cull in a Similar Way through Ionic Interactions, *Chem. Eur. J.*, 2021, **27**, 2798-2809.
58. C. J. Pike, M. J. Overman and C. W. Cotman, Amino-terminal Deletions Enhance Aggregation of  $\beta$ -Amyloid Peptides in Vitro(\*), *J. Biol. Chem.*, 1995, **270**, 23895-23898.
59. E. Cabrera, P. Mathews, E. Mezhericher, T. G. Beach, J. Deng, T. A. Neubert, A. Rostagno and J. Ghiso, A $\beta$  truncated species: Implications for brain clearance mechanisms and amyloid plaque deposition, *Biochim. Biophys. Acta*, 2018, **1864**, 208-225.
60. H. Kozłowski, M. Luczkowski, M. Remelli and D. Valensin, Copper, zinc and iron in neurodegenerative diseases (Alzheimer's, Parkinson's and prion diseases), *Coord. Chem. Rev.*, 2012, **256**, 2129-2141.
61. K. J. Barnham, C. L. Masters and A. I. Bush, Neurodegenerative diseases and oxidative stress, *Nat. Rev. Drug Discov.*, 2004, **3**, 205-214.
62. C. Cheignon, M. Tomas, D. Bonnefont-Rousselot, P. Faller, C. Hureau and F. Collin, Oxidative stress and the amyloid beta peptide in Alzheimer's disease, *Redox Biol.*, 2018, **14**, 450-464.
63. M. del Barrio, V. Borghesani, C. Hureau and P. Faller, in *Biometals in Neurodegenerative Diseases*, eds. A. R. White, M. Aschner, L. G. Costa and A. I. Bush, Academic Press, 2017, DOI: 10.1016/B978-0-12-804562-6.00014-2, pp. 265-281.
64. C. Hureau, in *Alzheimer's Disease: Recent Findings in Pathophysiology, Diagnostic and Therapeutic Modalities*, ed. T. Govindaraju, The Royal Society of Chemistry, 2022, DOI: 10.1039/9781839162732-00170, pp. 170-192.
65. M. Rana and A. K. Sharma, Cu and Zn interactions with A $\beta$  peptides: consequence of coordination on aggregation and formation of neurotoxic soluble A $\beta$  oligomers, *Metallomics*, 2019, **11**, 64-84.
66. K. P. Kepp, Alzheimer's disease: How metal ions define  $\beta$ -amyloid function, *Coord. Chem. Rev.*, 2017, **351**, 127-159.
67. K. P. Kepp, Bioinorganic chemistry of Alzheimer's disease, *Chem. Rev.*, 2012, **112**, 5193-5239.
68. N. T. Watt, I. J. Whitehouse and N. M. Hooper, The Role of Zinc in Alzheimer's Disease, *International Journal of Alzheimer's Disease*, 2011, **2011**, 971021.
69. C. Esmieu, S. Hostachy and C. Hureau, Cu(II) chelators: useful tools to reveal and control Cu(II) homeostasis and toxicity, *Coord. Chem. Rev.*, 2025, in revision.
70. E. Falcone and C. Hureau, Redox processes in Cu-binding proteins: the "in-between" states in intrinsically disordered peptides, *Chemical Society Reviews*, 2023, **52**, 6595-6600.
71. C. Cheignon, M. Jones, E. Atrián-Blasco, I. Kieffer, P. Faller, F. Collin and C. Hureau, Identification of key structural features of the elusive Cu–A $\beta$  complex that generates ROS in Alzheimer's disease, *Chemical Science*, 2017, **8**, 5107-5118.
72. J. H. Viles, Metal ions and amyloid fiber formation in neurodegenerative diseases. Copper, zinc and iron in Alzheimer's, Parkinson's and prion diseases, *Coord. Chem. Rev.*, 2012, **256**, 2271-2284.
73. M. G. M. Weibull, S. Simonsen, C. R. Oksbjerg, M. K. Tiwari and L. Hemmingsen, Effects of Cu(II) on the aggregation of amyloid- $\beta$ , *J. Biol. Inorg. Chem.*, 2019, **24**, 1197-1215.
74. P. Faller, C. Hureau and O. Berthoumieu, Role of Metal Ions in the Self-assembly of the Alzheimer's Amyloid- $\beta$  Peptide, *Inorg. Chem.*, 2013, **52**, 12193-12206.



75. V. Oliveri, Unveiling the Effects of Copper Ions in the Aggregation of Amyloidogenic Proteins, *Molecules*, 2023, **28**, 6446. Article Online  
DOI: 10.1039/D5QI00850F
76. S. Park, C. Na, J. Han and M. H. Lim, Methods for analyzing the coordination and aggregation of metal–amyloid- $\beta$ , *Metallomics*, 2023, **15**, mfac102.
77. V. Töugu, A. Karafin, K. Zovo, R. S. Chung, C. Howells, A. K. West and P. Palumaa, Zn(II)- and Cu(II)-induced non-fibrillar aggregates of amyloid- $\beta$  (1–42) peptide are transformed to amyloid fibrils, both spontaneously and under the influence of metal chelators, *J. Neurochem.*, 2009, **110**, 1784–1795.
78. A. Abelein, S. Ciofi-Baffoni, C. Mörmann, R. Kumar, A. Giachetti, M. Piccioli and H. Biverstål, Molecular Structure of Cu(II)-Bound Amyloid- $\beta$  Monomer Implicated in Inhibition of Peptide Self-Assembly in Alzheimer's Disease, *JACS Au*, 2022, **2**, 2571–2584.
79. Y. Tian, Q. Shang, R. Liang and J. H. Viles, Copper(II) Can Kinetically Trap Arctic and Italian Amyloid- $\beta$ 40 as Toxic Oligomers, Mimicking Cu(II) Binding to Wild-Type Amyloid- $\beta$ 42: Implications for Familial Alzheimer's Disease, *JACS Au*, 2024, **4**, 578–591.
80. D. Noy, I. Solomonov, O. Sinkevich, T. Arad, K. Kjaer and I. Sagi, Zinc-Amyloid  $\beta$  Interactions on a Millisecond Time-Scale Stabilize Non-fibrillar Alzheimer-Related Species, *JACS*, 2008, **130**, 1376–1383.
81. A. Abelein, A. Gräslund and J. Danielsson, Zinc as chaperone-mimicking agent for retardation of amyloid  $\beta$  peptide fibril formation, *Proc. Natl. Acad. Sci. U.S.A.*, 2015, **112**, 5407–5412.
82. M.-C. Lee, W.-C. Yu, Y.-H. Shih, C.-Y. Chen, Z.-H. Guo, S.-J. Huang, J. C. C. Chan and Y.-R. Chen, Zinc ion rapidly induces toxic, off-pathway amyloid- $\beta$  oligomers distinct from amyloid- $\beta$  derived diffusible ligands in Alzheimer's disease, *Sci. Rep.*, 2018, **8**, 4772.
83. F. Shen, D. Regmi, M. Islam, D. Raja Somu, V. Merk and D. Du, Effects of zinc and carnosine on aggregation kinetics of Amyloid- $\beta$ 40 peptide, *Biochemistry and Biophysics Reports*, 2022, **32**, 101333.
84. M. Lee, J. I. Kim, S. Na and K. Eom, Metal ions affect the formation and stability of amyloid  $\beta$  aggregates at multiple length scales, *Physical Chemistry Chemical Physics*, 2018, **20**, 8951–8961.
85. E. Atrian-Blasco, A. Conte-Daban and C. Hureau, Mutual interference of Cu and Zn ions in Alzheimer's disease: perspectives at the molecular level, *Dalton Trans.*, 2017, **46**, 12750–12759.
86. P. Gonzalez, K. Bossak, E. Stefaniak, C. Hureau, L. Raibaut, W. Bal and P. Faller, N-Terminal Cu-Binding Motifs (Xxx-Zzz-His, Xxx-His) and Their Derivatives: Chemistry, Biology and Medicinal Applications, *Chem. Eur. J.*, 2018, **24**, 8029–8041.
87. M. Mital, N. E. Wezynfeld, T. Frączyk, M. Z. Wiloch, U. E. Wawrzyniak, A. Bonna, C. Tumpach, K. J. Barnham, C. L. Haigh, W. Bal and S. C. Drew, A Functional Role for A $\beta$  in Metal Homeostasis? N-Truncation and High-Affinity Copper Binding, *Angew. Chem. Int. Ed.*, 2015, **54**, 10460–10464.
88. I. Sóvágó, K. Várnagy, N. Lihi and Á. Grenács, Coordinating properties of peptides containing histidyl residues, *Coord. Chem. Rev.*, 2016, **327–328**, 43–54.
89. I. Sóvágó, C. Kállay and K. Várnagy, Peptides as complexing agents: Factors influencing the structure and thermodynamic stability of peptide complexes, *Coord. Chem. Rev.*, 2012, **256**, 2225–2233.
90. T. Giuseppe, S. Cristina and M. Diego La, Peptides and their Metal Complexes in Neurodegenerative Diseases: from Structural Studies to Nanomedicine Prospects, *Current Medicinal Chemistry*, 2018, **25**, 715–747.
91. S. M. Hosseinpour Mashkani, D. P. Bishop, M. T. Westerhausen, P. A. Adlard and S. M. Golzan, Alterations in zinc, copper, and iron levels in the retina and brain of Alzheimer's disease patients and the APP/PS1 mouse model, *Metallomics*, 2024, **16**, mfae053.
92. B. Alies, A. Conte-Daban, S. Sayen, F. Collin, I. Kieffer, E. Guillon, P. Faller and C. Hureau, Zinc(II) Binding Site to the Amyloid- $\beta$  Peptide: Insights from Spectroscopic Studies with a Wide Series of Modified Peptides, *Inorg. Chem.*, 2016, **55**, 10499–10509.





93. B. Aliès, V. Borghesani, S. Noël, S. Sayen, E. Guillon, D. Testemale, P. Faller and C. Hureau, Mutations of Histidine 13 to Arginine and Arginine 5 to Glycine Are Responsible for Different Coordination Sites of Zinc(II) to Human and Murine Peptides, *Chem. Eur. J.*, 2018, **24**, 14233-14241.
94. E. Gaggelli, A. Janicka-Klos, E. Jankowska, H. Kozłowski, C. Migliorini, E. Molteni, D. Valensin, G. Valensin and E. Wiczerzak, NMR studies of the Zn<sup>2+</sup> interactions with rat and human beta-amyloid (1-28) peptides in water-micelle environment., *J. Phys. Chem. B.*, 2008, **112**, 100-109.
95. S. Zirah, S. A. Kozin, A. K. Mazur, A. Blond, M. Cheminant, I. Ségalas-Milazzo, P. Debey and S. Rebuffat, Structural changes of region 1-16 of the Alzheimer disease amyloid b-peptide upon zinc binding and in vitro aging, *J. Biol. Chem.*, 2006, **281**, 2151-2161.
96. C. Talmard, A. Bouzan and P. Faller, Zinc Binding to Amyloid-: Isothermal Titration Calorimetry and Zn Competition Experiments with Zn Sensors, *Biochemistry*, 2007, **46**, 13658-13666.
97. J. Danielsson, R. Pierattelli, L. Banci and A. Graslund, High-resolution NMR studies of the zinc-binding site of the Alzheimer's amyloid beta-peptide, *FEBS J.*, 2007, **274**, 46-59.
98. P. O. Tsvetkov, A. A. Kulikova, A. V. Golovin, Y. V. Tkachev, A. I. Archakov, S. A. Kozin and A. A. Makarov, Minimal Zn(2+) binding site of amyloid-β., *Biophys. J.*, 2010, **99**, L84-86.
99. C. D. Syme and J. H. Viles, Solution 1H NMR investigation of Zn<sup>2+</sup> and Cd<sup>2+</sup> binding to amyloid-beta peptide (Abeta) of Alzheimer's disease, *Biochim. Biophys. Acta*, 2006, **1764**, 246-256.
100. I. Zawisza, M. Rozga and W. Bal, Affinity of peptides (Aβ, APP, α-synuclein, PrP) for metal ions (Cu, Zn), *Coord. Chem. Rev.*, 2012, **256**, 2297-2307.
101. V. Minicozzi, F. Stellato, M. Comai, M. D. Serra, C. Potrich, W. Meyer-Klaucke and S. Morante, Identifying the Minimal Copper- and Zinc-binding Site Sequence in Amyloid-β; Peptides \*, *J. Biol. Chem.*, 2008, **283**, 10784-10792.
102. B. Aliès, G. LaPenna, S. Sayen, E. Guillon, C. Hureau and P. Faller, Insights into the Mechanisms of Amyloid Formation of ZnII-Ab11-28: pH-Dependent Zinc Coordination and Overall Charge as Key Parameters for Kinetics and the Structure of ZnII-Ab11-28 Aggregates, *Inorg. Chem.*, 2012, **51**, 7897-7902.
103. T. Kowalik-Jankowska, M. Ruta, K. Wiśniewska and L. Łankiewicz, Coordination abilities of the 1–16 and 1–28 fragments of β-amyloid peptide towards copper(II) ions: a combined potentiometric and spectroscopic study, *Journal of Inorganic Biochemistry*, 2003, **95**, 270-282.
104. J. W. Karr and V. A. Szalai, Role of Aspartate-1 in Cu(II) binding to the Amyloid-b peptide Alzheimer's disease, *J. Am. Chem. Soc.*, 2007, **129**, 3796-3797.
105. C. D. Syme, R. C. Nadal, S. E. Rigby and J. H. Viles, Copper binding to the amyloid-beta (Abeta) peptide associated with Alzheimer's disease: folding, coordination geometry, pH dependence, stoichiometry, and affinity of Abeta-(1-28): insights from a range of complementary spectroscopic techniques, *J. Biol. Chem.*, 2004, **279**, 18169-18177.
106. B. Aliès, H. Eury, C. Bijani, L. Rechinat, P. Faller and C. Hureau, pH-Dependent Cu(II) Coordination to Amyloid-β Peptide: Impact of Sequence Alterations, Including the H6R and D7N Familial Mutations, *Inorg. Chem.*, 2011, **50**, 11192-11201.
107. C. A. Damante, K. Osz, Z. Nagy, G. Pappalardo, G. Grasso, G. Impellizzeri, E. Rizzarelli and I. Sóvágó, The metal loading ability of beta-amyloid N-terminus: a combined potentiometric and spectroscopic study of copper(II) complexes with beta-amyloid(1-16), its short or mutated peptide fragments, and its polyethylene glycol (PEG)-ylated analogue., *Inorg. Chem.*, 2008, **47**, 9669-9683.
108. G. Arena and E. Rizzarelli, Zn(2+) Interaction with Amyloid-B: Affinity and Speciation, *Molecules*, 2019, **24**, 2796.
109. P. Faller, C. Hureau, P. Dorlet, P. Hellwig, Y. Coppel, F. Collin and B. Aliès, Methods and techniques to study the bioinorganic chemistry of metal-peptide complexes linked to neurodegenerative diseases, *Coord. Chem. Rev.*, 2012, **256**, 2381-2396.



110. L. Giachini, G. Veronesi, F. Francia, G. Venturoli and F. Boscherini, Synergic approach to XAFS analysis for the identification of most probable binding motifs for mononuclear zinc sites in metalloproteins, *Journal of Synchrotron Radiation*, 2010, **17**, 41-52. Article Online  
DOI: 10.1039/D5Q100850F
111. J. E. Penner-Hahn, Characterization of "spectroscopically quiet" metals in biology, *Coord. Chem. Rev.*, 2005, **249**, 161-177.
112. B. Alies, V. Pradines, I. Llorens-Alliot, S. Sayen, E. Guillon, C. Hureau and P. Faller, Zinc(II) modulates specifically amyloid formation and structure in model peptides, *J Biol Inorg Chem*, 2011, **16**, 333-340.
113. S. S. Hasnian and C. D. Garner, Characterization of metal centres in biological systems by X-ray absorption spectroscopy, *Progress in Biophysics and Molecular Biology*, 1987, **50**, 47-65.
114. P. Zimmermann, S. Peredkov, P. M. Abdala, S. DeBeer, M. Tromp, C. Müller and J. A. van Bokhoven, Modern X-ray spectroscopy: XAS and XES in the laboratory, *Coord. Chem. Rev.*, 2020, **423**, 213466.
115. S. Noël, S. Bustos Rodriguez, S. Sayen, E. Guillon, P. Faller and C. Hureau, Use of a new water-soluble Zn sensor to determine Zn affinity for the amyloid- $\beta$  peptide and relevant mutants, *Metallomics*, 2014, **6**, 1220-1222.
116. P. Faller and C. Hureau, Reproducibility Problems of Amyloid- $\beta$  Self-Assembly and How to Deal With Them, *Frontiers in Chemistry*, 2021, **8**.
117. A. R. Foley and J. A. Raskatov, Assessing Reproducibility in Amyloid  $\beta$  Research: Impact of A $\beta$  Sources on Experimental Outcomes, *ChemBioChem*, 2020, **21**, 2425-2430.
118. D. J. Lindberg, M. S. Wranne, M. Gilbert Gatty, F. Westerlund and E. K. Esbjörner, Steady-state and time-resolved Thioflavin-T fluorescence can report on morphological differences in amyloid fibrils formed by A $\beta$ (1-40) and A $\beta$ (1-42), *Biochemical and Biophysical Research Communications*, 2015, **458**, 418-423.
119. A. Kocyla, A. Pomorski and A. Krężel, Molar absorption coefficients and stability constants of metal complexes of 4-(2-pyridylazo)resorcinol (PAR): Revisiting common chelating probe for the study of metalloproteins, *Journal of Inorganic Biochemistry*, 2015, **152**, 82-92.
120. C. Cheignon, F. Collin, L. Sabater and C. Hureau, Oxidative Damages on the Alzheimer's Related-A $\beta$  Peptide Alters Its Ability to Assemble, *Antioxidants*, 2023, **12**, 472.
121. C. Na, M. Kim, G. Kim, Y. Lin, Y.-H. Lee, W. Bal, E. Nam and M. H. Lim, Distinct Aggregation Behavior of N-Terminally Truncated A $\beta$ 4-42 Over A $\beta$ 1-42 in the Presence of Zn(II), *ACS Chem. Neurosci.*, 2025, **16**, 732-744.
122. T. Weiffert, G. Meisl, P. Flagmeier, S. De, C. J. R. Dunning, B. Frohm, H. Zetterberg, K. Blennow, E. Portelius, D. Klenerman, C. M. Dobson, T. P. J. Knowles and S. Linse, Increased Secondary Nucleation Underlies Accelerated Aggregation of the Four-Residue N-Terminally Truncated A $\beta$ 42 Species A $\beta$ 5-42, *ACS Chem. Neurosci.*, 2019, **10**, 2374-2384.
123. Y. Xiao, B. Ma, D. McElheny, S. Parthasarathy, F. Long, M. Hoshi, R. Nussinov and Y. Ishii, A $\beta$ (1-42) fibril structure illuminates self-recognition and replication of amyloid in Alzheimer's disease, *Nature Structural & Molecular Biology*, 2015, **22**, 499-505.
124. E. Stefaniak and W. Bal, Cull Binding Properties of N-Truncated A $\beta$  Peptides: In Search of Biological Function, *Inorg. Chem.*, 2019, **58**, 13561-13577.
125. T. Frączyk and P. Cieplak, Neglected N-Truncated Amyloid- $\beta$  Peptide and Its Mixed Cu-Zn Complexes, *The Protein Journal*, 2022, **41**, 361-368.
126. A. J. Dear, G. Meisl, A. Šarić, T. C. T. Michaels, M. Kjaergaard, S. Linse and T. P. J. Knowles, Identification of on- and off-pathway oligomers in amyloid fibril formation, *Chem. Sci.*, 2020, **11**, 6236-6247.
127. S. J. C. Lee, E. Nam, H. J. Lee, M. G. Savellieff and M. H. Lim, Towards an understanding of amyloid- $\beta$  oligomers: characterization, toxicity mechanisms, and inhibitors, *Chem. Soc. Rev.*, 2017, **46**, 310-323.



128. R. Kaye and C. A. Lasagna-Reeves, Molecular Mechanisms of Amyloid Oligomers Toxicity, *J. Alzheimer's Dis.*, 2013, **33**, S67-S78. Article Online  
DOI: 10.1039/D5QI00850F
129. C. Esmieu, G. Ferrand, V. Borghesani and C. Hureau, Impact of N-Truncated A $\beta$  Peptides on Cu- and Cu(A $\beta$ )-Generated ROS: Cul Matters!, *Chemistry – A European Journal*, 2021, **27**, 1777-1786.
130. M. Newville, Larch: An Analysis Package for XAFS and Related Spectroscopies, *Journal of Physics: Conference Series*, 2013, **430**, 012007.



The authors state that the data are available in the Supporting Information and on request.

[View Article Online](#)  
DOI: 10.1039/D5QI00850F

